Was there an ocean between the North China-Qaidam and Tarim blocks connecting the Mongol-Okhotsk and Paleo-Tethys oceans?

Teng Wang[a], Yanan Zhou[a*], Douwe J.J. van Hinbergen[b*], Mark J. Dekkers[b], Zhenwei Chen[a], Ruiyang Chai[a, b], Dongmeng Zhang[a], Bitian Wei[c], Anliang Xiong[a], Dongwei Liu[a], Xin Cheng[a], Hanning Wu[a], Yunpeng Dong[a*]

a. State Key Laboratory of Continental Evolution and Early Life, Department of Geology, Northwest University, Xi'an, China
b. Department of Earth Science, Utrecht University, Utrecht, Netherlands
c. State Key Laboratory of Lithospheric and Environmental Coevolution, Institute of Geology and Geophysics, Chinese Academy of Sciences, Beijing 100029, China

*Corresponding authors:
Yanan Zhou, zhouyanan@nwu.edu.cn
Douwe van J.J. Hinbergen, D.J.J.vanHinsbergen@uu.nl
Yunpeng Dong, dongyp@nwu.edu.cn

Abstract

The tectonic history of the final amalgamation of Eurasia is puzzling: geological and paleomagnetic data yield contrasting interpretations. Paleomagnetism shows that the North China Block and the Qaidam Basin fragment, migrated northward by several thousand kilometers relative to Eurasia until the latest Jurassic-Early Cretaceous. If true, plate tectonic principles require that a North China-Eurasia plate boundary existed. To the north, this may be the Mongol-Okhotsk suture, which contains sparse Mesozoic marine sediments. To the west, an associated geological record remains unknown. Here,

we report for the first time an inclination shallowing-corrected pole from Lower Permian limestones of the Qaidam Basin passing both fold and reversal tests, that yields a northern hemisphere reversed direction of D = 32.2° ± 4.5° and I = -44.2° ± 5.1°, corresponding to a paleomagnetic pole at λ = 17.4°S and φ = 247.6°E (A_{95} = 4.0°, K = 12.0, N = 113). This indicates a post-early Permian Qaidam-Eurasia convergence of ~20° (> 2000 km) in latitude, like North China. When combined with existing paleomagneitc data, it shows that this convergence was mostly accommodated after the Triassic. The robustness of the paleomagnetic dataset calls for an explanation of a missing geological record of convergence. Continental crustal shortening invariably leads to high orogens. We therefore speculate that a cryptic Mesozoic oceanic suture exists between the Qaidam and Eurasia, whose remains may be buried below the Tarim Basin. How this boundary connected to the Mongol-Okhotsk suture and to the Tethyan sutures remains currently unresolved and warrants further investigation.

Keywords: Qaidam Basin, Early Permian, Paleomagnetism, East Asia

1. Introduction

Ocean basins that formed and were destroyed by subduction in the geological past are preserved as sutures (e.g., Şengör et al., 1993). A suture typically separates two continental blocks with distinct geological characteristics and histories; it may preserve a geological record of a complete or parts of a Wilson cycle, including stratigraphic packages of passive margins and the eventual ocean basin, thereby enabling reconstruction of their tectonic evolution (Wilson et al., 2019). However, the completeness of that history depends strongly on if, and how much rocks of the former ocean basin accreted. Non-accretionary sutures make little topography are easily covered by younger sediments or overthrusted, in which case their recognition may become challenging (van Hinsbergen and Schouten, 2021). Evidence for a 'cryptic' suture may then come from paleomagnetic data that demonstrate that continental fragments on either side of a fault underwent strongly contrasting paleolatitudinal motions that require major convergence (van Hinsbergen et al., 2012; Halls, 2015).

Such a geological phenomenon may exist in East Eurasia, where the geological and paleomagnetic data on the final assembly of east Asian continental blocks with Eurasia are surprisingly conflict (Wang et al., 2025). East Asia consists of several continental fragments, including Amuria, North China, South China, Qaidam, and Qiangtang, which are all separated by sutures that are Triassic or older (Dong et al., 2011; Eizenhöfer et al., 2014; Eizenhöfer and Zhao, 2018; Kapp and DeCelles, 2019). However, paleomagnetic data for this composite continent show that it migrated between the late Triassic and earliest Cretaceous by more than 20° (in the west) to 30° (in the east) in latitude, corresponding to > 2000-3000 km, relative to Siberia and Kazakhstan that formed the eastern part of Eurasia (Cogné et al., 2005; Van der Voo et al., 2015; Wang et al., 2025). Such major motions must have been accommodated by convergent plate boundary, but associated geological records are surprisingly sparse.

A widely-inferred candidate to have formed this plate is the present-day Mongol-Okhotsk suture (Donskaya et al., 2013; Van der Voo et al., 2015; Wang et al., 2022a; Zhao et al., 2025). However, Mesozoic marine rocks are sparse in this suture zone, and only found in eastern Siberia (Arzhannikova et al., 2023). To the east set, a suture is often mapped as the Mongol-Okhotsk suture, but with only Paleozoic marine accreted sediments, which ends in an orocline (Fig. 1; Windley et al., 2007). However, no geological record is found in the west to document the thousands of kilometers of northward movement of the block. Yet, such records must exist and would connect to the Mongol-Okhotsk suture, because the amalgamation of all blocks must satisfy the geometric constraints of a triple junction (McKenzie and Morgan, 1969).

Based on a Late Permian paleomagnetic pole from the Qaidam Basin, Wang et al. (2025) recently argued that a cryptic suture may be located between the Tarim and Qaidam Basins, even though no geological record of such a suture is known.

In this study, we test the robustness of this paleomagnetic arguments and report a new paleolatitude from the Lower Permian of the Qaidam Basin. Combined with previous data, we will evaluate the robustness of the paleomagnetic argument for major plate convergence between Qaidam and Eurasia in the late Paleozoic to early Mesozoic,

and evaluate previous proposals how and where this convergence may have been accommodated.

2. Geological setting and sampling

The study area is in the northern part of the Qaidam Basin (Fig. 1a), where Late Paleozoic and Mesozoic strata are well exposed (Fig. 1b). The Qaidam Basin overlies the Qaidam continental block that is separated by an early Paleozoic suture, reactivated by Cenozoic thrusts, from the North China Block to the northeast (Zuza et al., 2018). Cenozoic shortening was limited to ~150 km (van Hinsbergen et al., 2011), and during late Paleozoic and Mesozoic times, Qaidam was part of the same continent as North China (Wang et al., 2025). To the south, the Qaidam Basin is bounded by the East Kunlun orogen, an arc that formed above a north-dipping subduction zone that consumed the Paleotethys Ocean, which closed in the middle Triassic due to the collision of the Qiangtang Block (Fig.1) (Dong et al., 2018; Sun et al., 2022; Wang et al., 2022b).

In this study, we focus on the Lower Permian Zhabusagaxiu Formation characterized by tidal-flat and lagoonal depositional environments (Wang et al., 2022b). The formation is mainly composed of interbedded limestone and mudstone (Figs. 2a, b), with sandstone occurring locally. The Zhabusagaxiu Formation is assigned to the Cisuralian (298.5-274.4 Ma) based on the U-Pb ages of tuff layers near its base (Fig. 2c; Wang et al., 2022b; Liu and Qian, 2023) and the presence of abundant fusulinid fossils, particularly *pseudoschwagerina* and *spyroschwagerina* (Ma et al., 2020).

We collected a total of 299 oriented paleomagnetic limestone samples from 31 locations from the Lower Permian Zhabusagaxiu Formation in the Wanggaxiu area (37.00°N, 97.68°E) (Fig. 1b). These rocks were folded (Fig. 2a), allowing a paleomagnetic fold test. Core samples were collected by portable water-cooled gasoline-power drill, sampled across the stratigraphy to optimize the chance of sampling different spot readings of the paleomagnetic field (Figs. 2d, e, f; Gerritsen et al., 2022), and oriented using magnetic compass and sun compass when possible.

3. Methods

Each oriented core was cut into specimens of 2.2 cm in length. Anisotropy of magnetic susceptibility (AMS) measurements were conducted using an AGICO Kappabridge MFK-2 susceptibility meter at the Paleomagnetic Laboratory of Northwest University (Xi'an, China) to assess whether the magnetic minerals had been affected by tectonic deformation. Rock magnetic experiments were carried out at the Institute of Earth Environment, Chinese Academy of Sciences (Xi'an, China) and the Paleomagnetic Laboratory of Northwest University (Xi'an, China). Isothermal remanent magnetization (IRM) acquisition, back-field demagnetization, and thermal demagnetization of three-component IRMs (3-axis IRM) were performed using an ASC IM-10-30 pulse magnetizer, JR-6A magnetometer, TD-48 thermal demagnetizer, respectively. Hysteresis loops were measured with a MicroMag 3900 Vibrating Sample Magnetometer.

Thermal and alternating field (AF) demagnetization, as well as remanent magnetization measurement experiments, were conducted using a TD-48 thermal demagnetizer, D-2000 alternating field demagnetizer, and a 2G-755R superconducting magnetometer at the Paleomagnetic Laboratory of Northwest University (Xi'an, China), and an automatic magnetometer-AF demagnetization system (Mullender et al., 2016) at the Fort Hoofddijk Paleomagnetic Laboratory, Utrecht University (Utrecht, Netherlands). Paleomagnetic data analysis was performed using the online portal Paleomagnetism.org (Koymans et al., 2016, 2020). The demagnetization results were plotted on orthogonal vector diagrams (Zijderveld, 1967) and principal component analysis (Kirschvink, 1980) was applied to isolate remanence components with a maximum angular deviation (MAD) $< 15°$. Mean paleomagnetic directions were calculated using standard Fisher statistics (Fisher, 1953) and analyzed using the online portal Paleomagnetism.org (Koymans et al., 2016, 2020). All paleomagnetic data were recalculated to a common reference site (37.0°N, 97.7°E) to facilitate palaeolatitudinal comparisons and subsequent discussion of tectonic implications.

4. Results

4.1. Anisotropy of Magnetic Susceptibility

After tilt correction, the anisotropy of magnetic susceptibility (AMS) results show subhorizontal K_1 (D=302.8°, I=2.4°) and K_2 axes (D=212.8°, I=1.0°), and nearly vertical K_3 axis (D=100.6°, I=87.4°) (Fig. S1). These fabrics define a bedding-parallel magnetic foliation, consistent with post-depositional compaction, and further indicate that the primary sedimentary magnetic fabrics have not been significantly overprinted by later tectonic deformation.

4.2. Rock Magnetic Results

The acquisition IRM curves increase rapidly in low applied fields (less than 200 mT), and reach saturation by ~300 mT (Figs. 3a-3c). The backfield demagnetization of saturation IRM curves show a maximum remanence coercive force less than 100 mT (Fig. 3). The three-axis IRM curves show that low-coercivity components are dominant, and unblocks at ~560 ℃ - 580 ℃ (Figs. 3d-3f). From these collected results, we infer that magnetite is the main magnetic carrier in most of the volcanic rock samples.

All hysteresis loops are narrow and reach saturation at low applied fields (Fig. 4), indicating the dominance of low-coercivity ferrimagnetic grains. Hysteresis parameters plotted on the Day diagram fall within the single-domain to multidomain (SD–MD) mixing region (Fig. 4). This domain state is generally regarded as favorable for the preservation of primary remanent magnetization (Jackson and Swanson-Hysell, 2012).

Together, these observations infer that the magnetite as the main magnetic minerals which carried the natural remanent magnetization (NRM).

4.3. Paleomagnetic results and statistical analysis

Stepwise thermal and alternating-field (AF) demagnetization were performed to isolate the characteristic remanent magnetization (ChRM). A total of 113 specimens yielded interpretable magnetic signals with AF demagnetization, revealing two distinct remanence components (Figs. 5a-5g). In contrast, thermal demagnetization failed to resolve any coherent components, producing only scattered, noisy demagnetization

trajectories (Figs. 5h-5j). This failure is most likely attributable to thermally induced physicochemical alteration during heating, which commonly affects weakly magnetized rocks (e.g., Banerjee, 1981). A low-field component was mostly removed between the starting NRM and 20-25 mT and yielded a mean direction of D_g=11.9°, I_g=51.3°, K_g=7.0, A_{95g}=5.4° in geographic coordinates, and D_s=0.2°, I_s=27.0°, K_s=2.7, A_{95s}=10.3° after tilt correction (Figs. 6a and 6b). In geographic coordinates, this mean direction is like that of the recent geomagnetic field direction at sampling location (D_{RGF}=1.2°, I_{RGF}=53.1°) and is interpreted as a viscous remanent magnetization.

After removal of the low-field component, a stable high-field component was isolated between ~20-30 mT and ~50-130 mT (Figs. 5a-6g), which is interpreted as the ChRM. Its mean direction is D_g=26.4° ± 7.7°, I_g=-7.5° ± 15.1°, K_g=4.0, A_{95g}=7.6° *in situ*, and D_s=32.9°± 3.9°, I_s=-29.5°± 6.2°, K_s=13.4, A_{95s}=3.8° after tilt correction, in stratigraphic coordinates (Figs. 6c and 6d; Table S1). The A_{95} value in stratigraphic coordinates falls within the n-dependent reliability envelope of Deenen et al. (2011) (N=113, $A_{95min, max}$=1.8, 4.2), which means that it may be straightforwardly explained by paleosecular variation (PSV) alone. The ChRM of the Zhabusagaxiu Formation show both normal and reverse polarities and a bootstrapped reversal test shows that the X, Y, and Z axes of the mean directions between normal and reverse polarities of the ChRM are indistinguishable at a 95% confidence level (Tauxe et al., 2016), reflecting a positive reversal test (Fig. S2). Application of the Tauxe and Watson (1994) fold test yielded the highest τ1 value between 89% and 101%, indicating that the ChRM was acquired before folding (Fig. S3).

Paleomagnetic directions obtained from sedimentary rocks are commonly influenced by post-depositional compaction (e.g., Tauxe and Kent, 2004; Vaes et al., 2021). Therefore, correction for inclination shallowing is essential when interpreting paleomagnetic data from sedimentary rocks. Our results satisfied inclination correction criteria proposed by Vaes et al. (2021): (a) a sufficiently large sample size (N ≥ 80); (b) fulfillment of the Deenen et al. (2011) criteria, and (c) limited vertical-axis rotations within the dataset that do not exceed ~15°. In this study, we applied the elongation-inclination (E/I) method of Tauxe and Kent (2004). The correction applied yields a

flattening factor of 0.52 (Fig. 7) and increases the inclination from -29.5° to -44.2°. After E/I correction, the total of 113 specimens yielded an overall mean direction of D_s=32.2°± 4.5°, I_s=-44.2°± 5.1°, K_s=12.0, A_{95s}=4.0° in stratigraphic coordinates (Fig. 7), also satisfying the Deenen et al. (2011) criteria. We interpret this as a northern hemisphere, reverse direction, as expected because the section was deposited during the Kiaman reverse superchron (Ogg, 2020). The corresponding paleolatitude is 26.0° ± 4.0°N. Such results, however, indicate that the sampling locality subsequently underwent a significant counterclockwise (CCW) rotation. The subduction of the Paleo-Tethys Ocean led to the uplift of the Qaidam Basin, causing a depositional hiatus within the basin and transforming the South Qilian into a foreland basin (Xiao et al., 2021). Furthermore, the oblique nature of the Paleo-Tethys subduction induced strike-slip motion between the Qaidam and South Qilian regions (Wu et al., 2026). We suggest that this tectonic process was likely the primary cause of the observed rotation.

Finally, based on the rock magnetic results, the positive fold and reversal tests, and the presence of inclination shallowing that has been quantitatively corrected, we conclude that the limestones of the Zhabusagxiu Formation preserve a primary remanent magnetic signal and therefore provide a reliable basis for subsequent tectonic reconstructions.

5. Discussion

5.1. The paleogeographic location of the Qaidam Basin during Permian to Triassic

The online portals APWP-online.org (Vaes et al., 2024) and Paleomagnetism.org (Koymans et al., 2016, 2020) were used to compute and compare the latitudinal distances between our new paleomagnetic results for the Lower Permian of the Qaidam Block and the apparent polar wander path in Eurasian coordinates (Vaes et al., 2023) as well as with time-equivalent paleomagnetic poles of Tarim and North China (Table S2). During the Early Permian, all three blocks—Tarim, North China, and Qaidam—show significant latitudinal offsets relative to Eurasia (Figs. 8 and S4). The Tarim Basin was in its final approach to Eurasia and lying 6.9° ± 4.4° (~750 ± 500 km) south of Eurasia (Figs. 8 and S4a), accommodated along a well-documented Permian suture in the Tien

Shan (Xiao et al., 2013).

Our newly obtained paleomagnetic pole indicates that the Qaidam Basin was located 18.6° ± 3.9° southward relative to Eurasia in the Early Permian (Fig. S4c). This is similar to estimates of 20.0° ± 4.4°, and 19.5° ± 3.2° in the Early Permian, Late Permian, and Middle Triassic (Fig. S4c). Moreover, the Permian paleomagnetic results from the Qaidam Basin (Wang et al., 2025; Song et al., 2026; this study) are paleolatitudinally indistinguishable from the North China Block's paleolatitudes (Figs. 8 and S4d). This demonstrates that in early Permian times, Qaidam was still paleolatitudinally separated from its modern position relative to Tarim and Eurasia by 2000 km of lithosphere; perhaps more because the paleolongitudinal component of motion is unconstrained by paleomagnetic data. The Triassic data from Qaidam show that this convergence was accommodated after the Middle Triassic (Fig S4c; Wang et al., 2024). A key question in the final assembly of Eurasia is where this convergence was accommodated.

Part of this convergence is accommodated by intracontinental shortening of Asian crust. The ENE-WSE striking Altyn Tagh strike-slip fault system that currently separates the Qaidam Basin from Tarim accommodated ca. 400 kilometers of left-lateral strike-slip (Yin et al., 2002; Cowgill et al., 2003), which translates to a N-S convergent component of about 150 kilometers, or ~1.5° (van Hinsbergen et al., 2011). In addition, the Tien Shan fold-thrust belt underwent up to ~200 km of Neogene shortening, increasing westwards accommodating a ~7° clockwise rotation of Tarim relative to Eurasia (van Hinsbergen et al., 2011). At the longitude of our study area, this may add another 0.5° of paleolatitudinal convergence between Qaidam and Eurasia. Cenozoic displacements may thus account for ~2° of paleolatitudinal convergence, which is far too small to compensate for the paleolatitudinal separation of several thousand kilometers between the Qaidam Basin and Eurasia inferred form the Permian-Triassic paleomagnetic data.

5.2. A cryptic suture connecting the Mongol-Okhotsk Suture between the Qaidam and Tarim basins?

If Qaidam and North China were connected, as follows from Permian and Triassic paleomagnetic data as well as geological constraints (Zuza et al., 2018), then the large paleomagnetic database of North China suggests that most post-middle Triassic convergence between Qaidam and Eurasia was accommodated during the Jurassic and accomplished by early Cretaceous times (e.g., Ren et al., 2018; Zhao et al., 2020; Wang et al., 2022a). The absence of oceanic rocks younger than mid-Paleozoic in northeastern Tibet and Tarim, and younger than the Permian in the Tien Shan could suggest that convergence was accommodated within continental crust. To the north, convergence would have been accommodated by closure of the Mongol–Okhotsk Suture, which is often cited to close during the Late Jurassic to Early Cretaceous based on paleomagnetic evidence for convergence, and Jurassic magmatism on either side of the suture (Donskaya et al., 2013; Van der Voo et al., 2015; Yi and Meert, 2020; Zhao et al., 2025), even though post-Paleozoic oceanic rocks are not known from this suture zone. The convergence between North China/Qaidam and Siberia would then occur in a 'scissor-like' fashion, with a fully continental connection from North China through Qaidam and Tarim to Eurasia, and an oceanic basin still open until earliest Cretaceous time to the north.

However, this scenario still requires more than 2000 km of relative latitudinal motion between Qaidam and Eurasia, which must have been tectonically accommodated. Oceanic subduction has the potential to accommodate the wholesale disappearance of lithosphere into the mantle – in fact, this is the default mode: the subduction zones around the Pacific Plate only occasionally preserve accreted geological records of subducted lithosphere (van Hinsbergen and Schouten, 2021). Intracontinental convergence, on the other hand, invariably leads to major shortening and orogenic uplift. For instance, the Andes accommodated 100-400 km of shortening, varying along-strike (Schepers et al., 2017), and the Atlas Mountains of northwest Africa accommodated only ~40 km of shortening (Beauchamp et al., 1999), yet both form majestic mountain belts. The Tibetan Plateau accommodated ~1000 km of shortening (van Hinsbergen et al., 2011; Ma et al., 2014), only half of the 2000 km of post-middle Triassic Qaidam-Euraisa convergence. However, there is no record of

Triassic-Jurassic shortening between Qaidam and Eurasia. It seems thus implausible to assume that Qaidam had a direct continental connection to Eurasia by Triassic times.

It is surprising that there is no geological record of a former plate boundary, yet the robustness of the paleomagnetic database of Qaidam and the China Blocks suggests that it must have existed. Oceanic sutures maybe non-accretionary and may leave little topography – exemplified by the Mongol-Okhotsk suture that is widely cited as a late Jurassic-early Cretaceous suture zone accommodating 1000s of km convergence despite the absence of an accretionary or topographic record (Arzhannikova et al., 2023). However, while it is surprising that no record is known, we find it more likely that such a suture, as well as an associated magmatic arc, lies buried below sediments, or is overthrusted by post-Jurassic tectonic activity. Golonka (2007) suggested that this cryptic suture may be hidden in the Tien Shan, whereas Wang et al. (2025) speculated about a location in the Tarim Basin, or overthrusted by the NW Tibetan Plateau. Based on the absence of a major continental shortening record between Qaidam and Tarim, we hypothesize that Qaidam-Eurasia collision occurred in the late Jurassic or early Cretaceous, and that prior to this time, an ocean existed, which we speculate separated Qaidam and Tarim. To the north, it would have connected to the Mongol-Okhotsk Ocean, and to the south to the Tethys domain (Fig. 9).

Future systematic paleomagnetic work on Triassic and older stratigraphy of Mongolia and China, like performed in this study, may help to approximate the location of the zone where this convergence was accommodated. However, an additional avenue may be targeted field studies on the terminations of other, better-known suture zones that formed during the amalgamation of east Asia. Those Permo-Triassic sutures formed on either side of the cryptic convergence zone discussed here.

One such suture formed because of closure of the Paleo-Tethys Ocean (Fig. 1a). To the east of our inferred cryptic convergence zone, this suture formed during the Middle to Late Triassic, in the east as a result of continental collisions involving the North China Block and the South China Block, and in the west, into the Tibetan Plateau, due to the collision of the Qiangtang Block and Qaidam Block (Dong et al., 2011, 2018; Song et al., 2015; Huang et al., 2018; Metcalfe, 2021; Wei et al., 2023). To the southwest,

in the Pamirs, Afghanistan, and Iran, the Paleotethys Suture formed by collision of Gondwana-derived continental fragments with Eurasia during the Late Triassic (Schwab et al., 2004; Angiolini et al., 2013; Villarreal et al., 2020).

The other candidate suture is the Tien Shan-Solonker suture, which is often mapped from west of the Pamir to the Pacific Ocean (Fig. 1a). However, to the east of the cryptic convergence zone, the Solonker Suture formed in the Triassic between North China and Amuria and to the west (Eizenhöfer et al., 2014; Eizenhöfer and Zhao, 2018), the Tien Shan Suture formed in the Permian between the Tarim Block and Eurasia (Xiao et al., 2004, 2013). Careful mapping of the terminations of these sutures may lead to the field evidence that may shed light on how the final amalgamation of Eurasia was tectonically established.

6. Conclusions

In this study, we present new paleomagnetic data from Lower Permian limestones of the Qaidam Basin. Positive fold and reversal tests indicate that the magnetization is likely primary. After correcting for inclination shallowing, the paleomagnetic pole is D = 32.2° ± 4.5°, I = -44.2° ± 5.1°, λ = 17.4°S, φ = 247.6°E, A95 = 4.0°, K = 12.0, N = 113. These results confirm that the Qaidam Basin migrated with North China during the Permian and that both terranes moved northward relative to Tarim/Eurasia by over 2000 km after the Triassic. We therefore propose the existence of a cryptic Mesozoic oceanic suture between Qaidam and Eurasia, potentially buried beneath the Tarim Basin.

CRediT authorship contribution statement

Teng Wang: Writing-original draft, Visualization, Software, Methodology, Investigation, Formal analysis, Data curation, Conceptualization. **Yanan Zhou**: Investigation, Funding acquisition, Writing-review & editing. **Douwe J.J. van Hinsbergen**: Conceptualization, Writing-review & editing. **Mark J. Dekkers**: Methodology, Writing-review & editing. **Zhenwei Chen**: Investigation, Data curation. **Ruiyang Chai**: Investigation, Data curation. **Dongmeng Zhang**: Investigation. **Bitian Wei**: Investigation. **Anliang Xiong**: Investigation. **Dongwei Liu**: Investigation. **Xin**

Cheng: Investigation. **Hanning Wu**: Investigation. **Yunpeng Dong**: Writing-review & editing.

Declaration of competing interest

The authors declare that they do have no competing financial interests or personal relationships that could have influenced the work reported in this paper.

Acknowledgement

This research was supported by the National Natural Science Foundation of China (Grants 42372251).

References

Angiolini, L., Zanchi, A., Zanchetta, S., Nicora, A., Vezzoli, G., 2013. The Cimmerian geopuzzle: New data from South Pamir. Terra Nova 25, 352-360. https://doi.org/10.1111/ter.12045

Arzhannikova, A.V., Demonterova, E.I., Sizov, A.V., Jolivet, M., Mikheeva, E.A., Ivanov, A.V., Arzhannikov, S.G., Khubanov, V.B., 2023. Early Cretaceous topographic evolution associated with the collapse of the Mongol-Okhotsk orogen in Western Transbaikalia: An integrated analysis. Int. Geol. Rev. 65 (15), 2348-2369. https://doi.org/10.1080/00206814.2022.2139296

Banerjee, S.K., 1981. Experimental methods of rock magnetism and paleomagnetism. Adv. Geophys. 23, 25–99. https://doi.org/ 10.1016/S0065-2687(08)60330-1

Beauchamp, W., Allmendinger, R.W., Barazangi, M., Demnati, A., El Alji, M., Dahmani, M., 1999. Inversion tectonics and the evolution of the High Atlas Mountains, Morocco, based on a geological-geophysical transect. Tectonics 18 (2), 163-184. https://doi.org/10.1029/1998TC900015

Cogné, J.P., Kravchinsky, V.A., Halim, N., Hankard, F., 2005. Late Jurassic-Early Cretaceous closure of the Mongol-Okhotsk Ocean demonstrated by new Mesozoic palaeomagnetic results from the Trans-Baikal area (SE Siberia). Geophys. J. Int. 163 (2), 813-832. https://doi.org/10.1111/j.1365-246X.2005.02782.x

Cowgill, E., Yin, A., Harrison, T.M., Wang, X.-F., 2003. Reconstruction of the Altyn Tagh fault based on U-Pb geochronology: Role of back thrusts, mantle sutures, and heterogeneous crustal strength in forming the Tibetan Plateau. J. Geophys. Res. Solid Earth 108 (B7), 2346. https://doi.org/10.1029/2002JB002080

Deenen, M.H.L., Langereis, C.G., van Hinsbergen, D.J.J., Biggin, A.J., 2011. Geomagnetic secular variation and the statistics of palaeomagnetic directions. Geophys. J. Int. 186 (2), 509-520. https://doi.org/10.1111/j.1365-246X.2011.05050.x

Dong, Y., He, D., Sun, S., Liu, X., Zhou, X., Zhang, F., Yang, Z., Cheng, B., Zhao, G., Li, J., 2018. Subduction and accretionary tectonics of the East Kunlun orogen, western segment of the

Central China Orogenic System. Earth-Sci. Rev. 186, 231-261. https://doi.org/10.1016/j.earscirev.2017.12.006

Dong, Y., Zhang, G., Neubauer, F., Liu, X., Genser, J., Hauzenberger, C., 2011. Tectonic evolution of the Qinling orogen, China: Review and synthesis. J. Asian Earth Sci. 41, 213-237. https://doi.org/ 10.1016/j.jseaes.2011.03.002

Donskaya, T., Gladkochub, D., Mazukabzov, A., Ivanov, A., 2013. Late Paleozoic-Mesozoic subduction-related magmatism at the southern margin of the Siberian continent and the 150 million-year history of the Mongol-Okhotsk Ocean. J. Asian Earth Sci. 62, 79-97. hhttps://doi.org/10.1016/j.jseaes.2012.07.023

Eizenhöfer, P.R., Zhao, G., 2018. Solonker Suture in East Asia and its bearing on the final closure of the eastern segment of the Palaeo-Asian Ocean. Earth-Sci. Rev. 186, 153-172. https://doi.org/10.1016/j.earscirev.2017.09.010

Eizenhöfer, P.R., Zhao, G., Zhang, J., Sun, M., 2014. Final closure of the Paleo-Asian Ocean along the Solonker suture zone: Constraints from geochronological and geochemical data of Permian volcanic and sedimentary rocks. Tectonics 33 (4), 441-463. https://doi.org/10.1002/2013TC003357

Fisher, R.A., 1953. Dispersion on a sphere. Proc. R. Soc. Lond. A 217 (1130), 295-305. https://doi.org/10.1098/rspa.1953.0064

Gerritsen, D., Vaes, B., van Hinsbergen, D.J.J., 2022. Influence of data filters on the position and precision of paleomagnetic poles: What is the optimal sampling strategy? Geochem. Geophys. Geosyst. 23 (4), e2021GC010269. https://doi.org/10.1029/2021GC010269

Golonka, J., 2007. Late Triassic and Early Jurassic palaeogeography of the world. Palaeogeogr. Palaeoclimatol. Palaeoecol. 244 (1-4), 297-307. https://doi.org/10.1016/j.palaeo.2006.06.041

Halls, H.C., 2015. Paleomagnetic evidence for ~4000 km of crustal shortening across the 1 Ga Grenville orogen of North America. Geology 43 (12), 1051-1054. https://doi.org/10.1130/G37188.1

Huang, B., Yan, Y., Piper, J.D.A., Zhang, D., Yi, Z., Yu, S., Zhou, T., 2018. Paleomagnetic constraints on the paleogeography of the East Asian blocks during Late Paleozoic and Early Mesozoic times. Earth-Sci. Rev. 186, 8-36. https://doi.org/10.1016/j.earscirev.2018.02.004

Jackson, M., Swanson-Hysell, N.L., 2012. Rock magnetism of remagnetized carbonate rocks: Another look. Geol. Soc. Lond. Spec. Publ. 371, 229–251. https://doi.org/10.1144/SP371.3

Kapp, P., DeCelles, P.G., 2019. Mesozoic-Cenozoic geological evolution of the Himalayan-Tibetan orogen and working tectonic hypotheses. Am. J. Sci. 319 (3), 159-254. https://doi.org/10.2475/03.2019.01

Kirschvink, J.L., 1980. The least-squares line and plane and the analysis of palaeomagnetic data. Geophys. J. R. Astron. Soc. 62 (3), 699-718. https://doi.org/10.1111/j.1365-246X.1980.tb02601.x

Koymans, M.R., Langereis, C.G., Pastor-Gal á n, D., van Hinsbergen, D.J.J., 2016. Paleomagnetism.org: An online multi-platform open source environment for paleomagnetic data analysis. Comput. Geosci. 93, 127-137. https://doi.org/10.1016/j.cageo.2016.05.007

Koymans, M., van Hinsbergen, D.J.J., Pastor-Galán, D., Vaes, B., Langereis, C., 2020. Towards FAIR paleomagnetic data management through Paleomagnetism.org 2.0. Geochem. Geophys. Geosyst. 21 (2), e2019GC008838. https://doi.org/10.1029/2019GC008838

Liu, J., Qian, T., 2023. Discovery of Permian tuff from the northern margin of the Qaidam Basin and its geological implications. J. Geomech. 29(02), 290-300. (In Chinese with English abstract)

Ma, L., Jiang, W., Xiao, Z., Li, Z., Peng, B., Hu, J., Dong, M., 2020. Discussion on the depositional timing of the Zhabusagaxiu formation in the eastern Qaidam Basin, China. J. Geomech. 26, 961-972. (In Chinese with English abstract)

Ma, Y., Yang, T., Yang, Z., Zhang, S., Wu, H., Li, H., Li, H., Chen, W., Zhang, J., Ding, J., 2014. Paleomagnetism and U-Pb zircon geochronology of Lower Cretaceous lava flows from the western Lhasa terrane: new constraints on the India-Asia collision process and intracontinental deformation within Asia. J. Geophys. Res. Solid Earth 119 (10), 7404-7424. https://doi.org/10.1002/2014JB011362

McKenzie, D.P., Morgan, W., 1969. Evolution of triple junctions. Nature 224, 125-133. https://doi.org/10.1038/224125a0

Metcalfe, I., 2021. Multiple Tethyan ocean basins and orogenic belts in Asia. Gondwana Res. 100, 87-130. https://doi.org/10.1016/j.gr.2021.01.012

Mullender, T.A., Frederichs, T., Hilgenfeldt, C., de Groot, L.V., Fabian, K., Dekkers, M.J., 2016. Automated paleomagnetic and rock magnetic data acquisition with an in-line horizontal "2 G " system. Geochem. Geophys. Geosyst. 17 (9), 3546-3559. https://doi.org/10.1002/2016GC006436

Ogg, J.G., 2020. Geomagnetic polarity time scale. Geol. Time Scale 2020, Elsevier 1, 159-192. https://doi.org/10.1016/B978-0-12-824360-2.00005-X

Ren, Q., Zhang, S., Hou, M., Zheng, D., Wu, H., Yang, T., Li, H., Chen, A., Ogg, J.G., 2025. Continental drift triggered the Early Permian aridification of North China. Nat. Commun. 16, 384. https://doi.org/10.1038/s41467-024-55804-8

Ren, Q., Zhang, S., Wu, Y., Yang, T., Gao, Y., Turbold, S., Zhao, H., Wu, H., Li, H., Fu, H., 2018. New Late Jurassic to Early Cretaceous paleomagnetic results from North China and southern Mongolia and their implications for the evolution of the Mongol-Okhotsk suture. J. Geophys. Res. Solid Earth 123 (12), 10370-10398. https://doi.org/10.1029/2018JB016703

Schepers, G., van Hinsbergen, D.J., Spakman, W., Kosters, M.E., Boschman, L.M., McQuarrie, N., 2017. South-American plate advance and forced Andean trench retreat as drivers for transient flat subduction episodes. Nat. Commun. 8, 15249. https://doi.org/10.1038/ncomms15249

Schwab, M., Ratschbacher, L., Siebel, W., McWilliams, M., Minaev, V., Lutkov, V., Chen, F., Stanek, K., Nelson, B., Frisch, W., 2004. Assembly of the Pamirs: age and origin of magmatic belts from the southern Tien Shan to the southern Pamirs and their relation to Tibet. Tectonics 23 (4), TC4002. https://doi.org/10.1029/2003TC001583

Şengör, A., Natal'In, B., Burtman, V., 1993. Evolution of the Altaid tectonic collage and Palaeozoic crustal growth in Eurasia. Nature, 364, 299-307. https://doi.org/10.1038/364299a0

Song, P., Ding, L., Li, Z., Lippert, P.C., Yang, T., Zhao, X., Fu, J., Yue, Y., 2015. Late Triassic paleolatitude of the Qiangtang block: implications for the closure of the Paleo-Tethys Ocean. Earth Planet. Sci. Lett. 424, 69-83. https://doi.org/10.1016/j.epsl.2015.05.020

Song, P., Ding, L., Zhang, L., Wu, C., Duan, X., Yue, Y., Xie, J., 2026. Defining the main Paleo-Tethys suture in Tibet: first Permian paleomagnetic insights from the Eastern Kunlun Range. Earth Planet. Sci. Lett. 681, 119925. https://doi.org/10.1016/j.epsl.2026.119925

Sun, J., Dong, Y., Ma, L., Chen, S., Jiang, W., 2022. Devonian to Triassic tectonic evolution and basin transition in the East Kunlun-Qaidam area, northern Tibetan Plateau: constraints from stratigraphy and detrital zircon U-Pb geochronology. GSA Bull. 134 (7-8), 1967-1993. https://doi.org/10.1130/B36147.1

Tauxe, L., Kent, D.V., 2004. A simplified statistical model for the geomagnetic field and the detection of shallow bias in paleomagnetic inclinations: was the ancient magnetic field dipolar? Geophys. Monogr. 145, 101-115. https://doi.org/10.1029/145GM08

Tauxe, L., Watson, G., 1994. The fold test: an eigen analysis approach. Earth Planet. Sci. Lett. 122 (304), 331-341. https://doi.org/10.1016/0012-821X(94)90006-X

Tauxe, L., Shaar, R., Jonestrask, L., Swanson-Hysell, N.L., Minnett, R., Koppers, A.A.P., Constable, C.G., Jarboe, N., Gaastra, K., Fairchild, L., 2016. PmagPy: software package for paleomagnetic data analysis and a bridge to the Magnetics Information Consortium (MagIC) Database. Geochem. Geophys. Geosyst. 17 (6), 2450-2463. https://doi.org/10.1002/2016GC006307

Vaes, B., Li, S., Langereis, C.G., van Hinsbergen, D.J., 2021. Reliability of palaeomagnetic poles from sedimentary rocks. Geophys. J. Int. 225 (1), 1281-1303. https://doi.org/10.1093/gji/ggab016

Vaes, B., van Hinsbergen, D.J., van de Lagemaat, S.H., van der Wiel, E., Lom, N., Advokaat, E.L., Boschman, L.M., Gallo, L.C., Greve, A., Guilmette, C., 2023. A global apparent polar wander path for the last 320 Ma calculated from site-level paleomagnetic data. Earth-Sci. Rev. 245, 104547. https://doi.org/10.1016/j.earscirev.2023.104547

Vaes, B., van Hinsbergen, D., Paridaens, J., 2024. APWP-online.org: a global reference database and open-source tools for calculating apparent polar wander paths and relative paleomagnetic displacements. Tektonika 2 (1), 174-189. https://doi.org/10.55575/tektonika2024.2.1.44

Van der Voo, R., van Hinsbergen, D.J., Domeier, M., Spakman, W., Torsvik, T.H., 2015. Latest Jurassic–earliest Cretaceous closure of the Mongol-Okhotsk Ocean: a paleomagnetic and seismological-tomographic analysis. GSA Spec. Pap. 513, 589-606. https://doi.org/10.1130/2015.2513(19)

van Hinsbergen, D.J., Schouten, T.L., 2021. Deciphering paleogeography from orogenic architecture: constructing orogens in a future supercontinent as thought experiment. Am. J. Sci. 321 (6), 955-1031. https://doi.org/10.2475/06.2021.09

van Hinsbergen, D.J., Kapp, P., Dupont-Nivet, G., Lippert, P.C., DeCelles, P.G., Torsvik, T.H., 2011. Restoration of Cenozoic deformation in Asia and the size of Greater India. Tectonics 30 (5), TC5003. https://doi.org/10.1029/2011TC002908

van Hinsbergen, D.J., Lippert, P.C., Dupont-Nivet, G., McQuarrie, N., Doubrovine, P.V., Spakman, W., Torsvik, T.H., 2012. Greater India Basin hypothesis and a two-stage Cenozoic collision between India and Asia. Proc. Natl. Acad. Sci. USA 109 (20), 7659-7664. https://doi.org/10.1073/pnas.1117262109

Villarreal, D.P., Robinson, A.C., Carrapa, B., Worthington, J., Chapman, J.B., Oimahmadov, I., Gadoev, M., MacDonald, B., 2020. Evidence for Late Triassic crustal suturing of the Central and Southern Pamir. J. Asian Earth Sci. X 3, 100024. https://doi.org/10.1016/j.jaesx.2019.100024

Wang, B., Huang, B., Yang, Z., Zhang, G., Liu, X., Duan, L., Armstrong, R.A., Meng, Q., 2024.

Palaeomagnetic results from Early Mesozoic strata in the Qaidam Basin and their implications for the formation of the Northern China Domain. Geophys. J. Int., 236 (3), 1621-1635. https://doi.org/10.1093/gji/ggad496

Wang, T., Tong, Y., Xiao, W., Guo, L., Windley, B.F., Donskaya, T., Li, S., Tserendash, N., Zhang, J., 2022a. Rollback, scissor-like closure of the Mongol-Okhotsk Ocean and formation of an orocline: magmatic migration based on a large archive of age data. Natl. Sci. Rev. 9 (5), nwab210. https://doi.org/10.1093/nsr/nwab210

Wang, T., Zhou, Y., He, W., He, L., Cheng, X., Deng, X., Zhang, D., Wei, B., Jiang, N., Wu, H., 2022b. Provenance change in Carboniferous-early Permian sedimentary successions in the North Qaidam tectonic belt, northern Tibetan Plateau: implications for the Kunlun oceanic plate subduction process. J. Asian Earth Sci. 240, 105434. https://doi.org/10.1016/j.jseaes.2022.105434

Wang, T., Zhou, Y., van Hinsbergen, D.J.J., Sun, J., Cheng, X., Chai, R., Xu, S., Wang, P., Wu, H., 2025. Paleomagnetic evidence for a Late Permian Qaidam–North China connection, and the cryptic final Mesozoic intra-Asian suture. J. Geophys. Res. Solid Earth 130 (8), e2025JB031123. https://doi.org/10.1029/2025JB031123

Wei, B., Cheng, X., Domeier, M., Zhou, Y., Chen, Q., Jiang, N., Xing, L., Zhang, D., Li, T., Liu, F., 2023. Paleomagnetism of Late Triassic volcanic rocks from the South Qiangtang Block, Tibet: constraints on Longmuco–Shuanghu Ocean closure in the Paleo-Tethys Realm. Geophys. Res. Lett. 50 (19), e2023GL104759. https://doi.org/10.1029/2023GL104759

Wei, B., Yang, X., Cheng, X., Domeier, M., Wu, H., Kravchinsky, V.A., Zhou, Y., Jiang, N., Wu, Y., Huo, F., 2020. An absolute paleogeographic positioning of the early Permian Tarim large igneous province. J. Geophys. Res. Solid Earth 125 (5), e2019JB019111. https://doi.org/10.1029/2019JB019111

Wilson, R.W., Houseman, G.A., Buiter, S., McCaffrey, K.J., Doré, A.G., 2019. Fifty years of the Wilson Cycle concept in plate tectonics: an overview. Geol. Soc. Lond. Spec. Publ. 470, 9781786203878. https://doi.org/10.1144/SP470

Windley, B.F., Alexeiev, D., Xiao, W., Kröner, A., Badarch, G., 2007. Tectonic models for accretion of the Central Asian Orogenic Belt. J. Geol. Soc. 164 (1), 31-47. https://doi.org/10.1144/0016-76492006-022

Wu, Y., Zhang, J., Angiboust, S., Zhang, B., Mao, X., Teng, X., 2026. Triassic sinistral transpression of the overriding plate in NE Tibet driven by oblique subduction of the Paleo-Tethys. Tectonics 45 (1), e2025TC009154. https://doi.org/10.1029/2025TC009154

Xiao, A.C., Yu, L., Xiong, G.Y., Zhang, J.Y., Zhang, Y.X., Wu, L., Zhao, H.F., Qin, S.H., 2021. Triassic retroarc foreland basin in southern Qilian area: evidence from sedimentary filling and tectonics. Acta Petrolog. Sin. 37, 2385-2400. (In Chinese with English abstract)

Xiao, W.J., Zhang, L.C., Qin, K.Z., Sun, S., Li, J.L., 2004. Paleozoic accretionary and collisional tectonics of the Eastern Tianshan (China): implications for the continental growth of central Asia. Am. J. Sci. 304 (4), 370-395. https://doi.org/10.2475/ajs.304.4.370

Xiao, W., Windley, B.F., Allen, M.B., Han, C., 2013. Paleozoic multiple accretionary and collisional tectonics of the Chinese Tianshan orogenic collage. Gondwana Res. 23 (4), 1316-1341. https://doi.org/10.1016/j.gr.2012.01.012

Xu, W., Song, B., Shi, J., Li, Y., Wang, B., Ye, X., Han, X., Xu, H., Zhang, Y., Zhang, H., Sun, Z., 2025. New Permian paleomagnetic and geochronologic results from the Alxa Block:

constraints on its tectonic affinity and the closure of Paleo-Asian Ocean. Geophys. Res. Lett. 52 (20), e2025GL116752. https://doi.org/10.1029/2025GL116752

Yi, Z., Meert, J.G., 2020. A closure of the Mongol-Okhotsk Ocean by the Middle Jurassic: reconciliation of paleomagnetic and geological evidence. Geophys. Res. Lett. 47 (15), e2020GL088235. https://doi.org/10.1029/2020GL088235

Yin, A., Rumelhart, P., Butler, R., Cowgill, E., Harrison, T., Foster, D., Ingersoll, R., Zhang, Q., Zhou, X. Q., Wang, X. F., Hanson, A., Raza, A., 2002. Tectonic history of the Altyn Tagh fault system in northern Tibet inferred from Cenozoic sedimentation. GSA Bull. 114 (10), 1257-1295. https://doi.org/10.1130/0016-7606(2002)114%3C1257:THOTAT%3E2.0.CO;2

Zhang, D., Huang, B., Zhao, J., Meert, J.G., Zhang, Y., Liang, Y., Bai, Q., Zhou, T., 2018. Permian paleogeography of the eastern CAOB: paleomagnetic constraints from volcanic rocks in central eastern Inner Mongolia, NE China. J. Geophys. Res. Solid Earth 123 (40), 2559-2582. https://doi.org/10.1002/2018JB015614

Zhao, P., Appel, E., Xu, B., 2020. An inclination shallowing-corrected Early Triassic paleomagnetic pole for the North China Craton: implication for the Mesozoic geography of Proto-Asia. J. Geophys. Res. Solid Earth 125 (10), e2020JB019489. https://doi.org/10.1029/2020JB019489

Zhao, P., Hou, Y., Jia, Z., Appel, E., Deng, C., Chen, Y., 2025. A possible Late Jurassic final closure of the Mongol-Okhotsk Ocean in its eastern segment: constraints from new paleomagnetic investigations. J. Geophys. Res. Solid Earth 130 (7), e2024JB030741. https://doi.org/10.1029/2024JB030741

Zhao, X., Robert, S.C., Zhou, Y., Wu, H., Wang, J., 1990. New paleomagnetic results from northern China: collision and suturing with Siberia and Kazakhstan. Tectonophysics 181 (1-4), 43-81. https://doi.org/10.1016/0040-1951(90)90008-V

Zhou, T.H., Huang, B.C., Jia, S.F., Liang, Y.L., Zhang, D.H., Zhao, Q., Zhang, Y., Yan, Y.G., 2018. Paleomagnetic inclination shallowing in Lower Triassic Liujiagou Formation from Qinshui Basin, North China Block. Acta Sci. Nat. Univ. Pekin., 54 (3), 521-534. (In Chinese with English abstract)

Zijderveld, J.D.A., 1967. AC demagnetization of rocks: analysis of results. In: Collinson, D.W., Creer, K.M., Runcorn, S.K. (Eds.), Methods in Paleomagnetism, Elsevier 3, 254-286. https://doi.org/10.1016/B978-1-4832-2894-5.50049-5

Zuza, A.V., Wu, C., Reith, R.C., Yin, A., Li, J., Zhang, J., Zhang, Y., Wu, L., Liu, W., 2018. Tectonic evolution of the Qilian Shan: An early Paleozoic orogen reactivated in the Cenozoic. GSA Bull. 130 (5-6), 881-925. https://doi.org/10.1130/B31721.1

Figures

Figure 1. Geological map of the study area. (1) Simplified geotectonic framework of East Asia showing the location of the study area; (2) Geological sketch map of the study area in Northern Qaidam Basin.

Figure 2. Representative field photos of sampling locations. (a, b) Interbedded limestone and mudstone; (c) Tuff layers with U-Pb ages in the bottom of the Zhabusagaxiu Formation; (d-f) Paleomagnetic drill holes, illustrating the sampling strategy. The building in Figure 2a is approximately 3 m tall; the geologist in Figure 2b and 2c is approximately 1.85 m; the geological hammer in Figures 2d, 2e, and 2f is 35 cm in length.

Figure 3. Rock magnetic analyses of samples from the Zhabusagaxiu Formation. (a–c) Isothermal remanent magnetization (IRM) acquisition curves and backfield demagnetization of saturation IRM curves of representative samples; (d–f) Thermal demagnetization of three-axis IRM curves of representative samples.

Figure 4. Hysteresis loops and Day plot of Zhabusagaxiu Formation limestones.

Figure 5. Representative demagnetization diagrams for specimens from the Zhabusagaxiu Formation limestones in stratigraphic coordinates. Filled circles represent the horizontal projections, open circles represent the vertical projections. NRM is the natural remanent magnetization.

Figure 6. Paleomagnetic results from Zhabusagaxiu Formation. (a and b) Equal-area plots of the low-field component before and after tilt correction; (c and d) Equal-area plots of the high-field component before and after tilt correction.

Figure 7. Elongation/inclination (E/I) correction (Tauxe and Kent, 2004) applied to the ChRMs.

Figure 8. Paleolatitudinal comparison of Eurasia, North China, Tarim, and Qaidam during the

637 Permo-Triassic. The paleolatitude evolution was calculated and drawn using the online tools
638 APWP-Online.org (Vaes et al., 2024) and paleomagnetism.org (Koymans et al., 2016, 2020),
639 respectively.
640
641 **Figure 9.** Schematic paleogeographic reconstruction of the East Asian blocks, Laurussia, Siberia,
642 and Gondwana at ca .290 Ma. The Qaidam Block is positioned according to the data in this study.
643 Amuria, South China, the Tethyan oceans, and the major continents follow reconstructions of
644 Torsvik and Cocks (2017), Song et al. (2017), Huang et al. (2018), Ren et al. (2020), van Hinsbergen
645 et al. (2020), and Advokaat and van Hinsbergen. (2024), placed in the paleomagnetic reference
646 frame of Vaes et al. (2023).
647

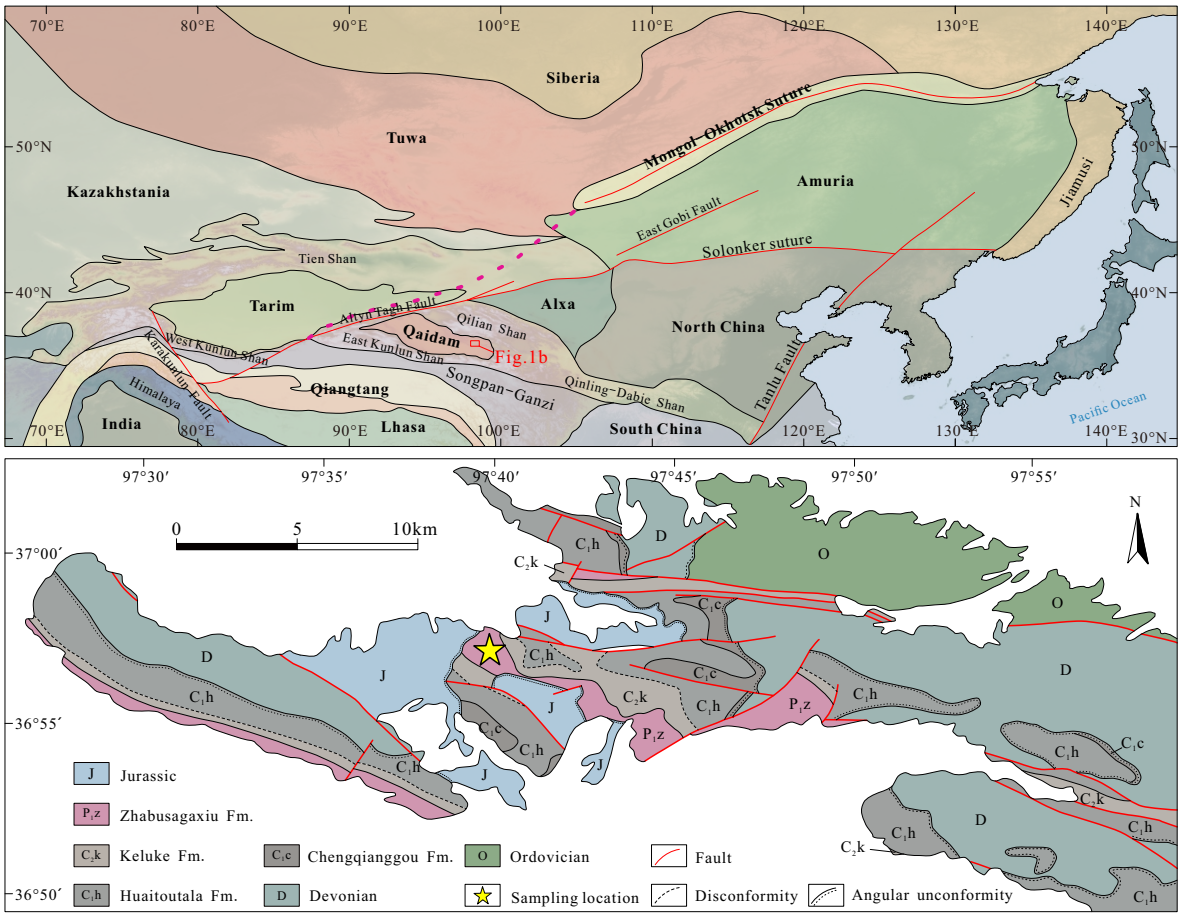
70°E
80°E
90°E
100°E
110°E
120°E
130°E
140°E
50°N
40°N
30°N
Siberia
Tuwa
Mongol–Okhotsk Suture
Kazakhstania
Amuria
Jiamusi
East Gobi Fault
Solonker suture
Tien Shan
Tarim
Alxa
North China
Altyn Tagh Fault
Qilian Shan
Qaidam
Fig.1b
West Kunlun Shan
East Kunlun Shan
Songpan–Ganzi
Qinling–Dabie Shan
Tanlu Fault
Karakuntun Fault
Himalaya
Qiangtang
India
Lhasa
South China
Pacific Ocean
97°30′
97°35′
97°40′
97°45′
97°50′
97°55′
37°00′
36°55′
36°50′
0
5
10km
N
C1h
C2k
D
O
J
C1c
P1z
Jurassic
Zhabusagaxiu Fm.
Keluke Fm.
Chengqianggou Fm.
Ordovician
Fault
Huaitoutala Fm.
Devonian
Sampling location
Disconformity
Angular unconformity


a
b
c
293±3 Ma (Wang et al., 2022)
295±2 Ma (Liu and Qian, 2023)
d
e
f

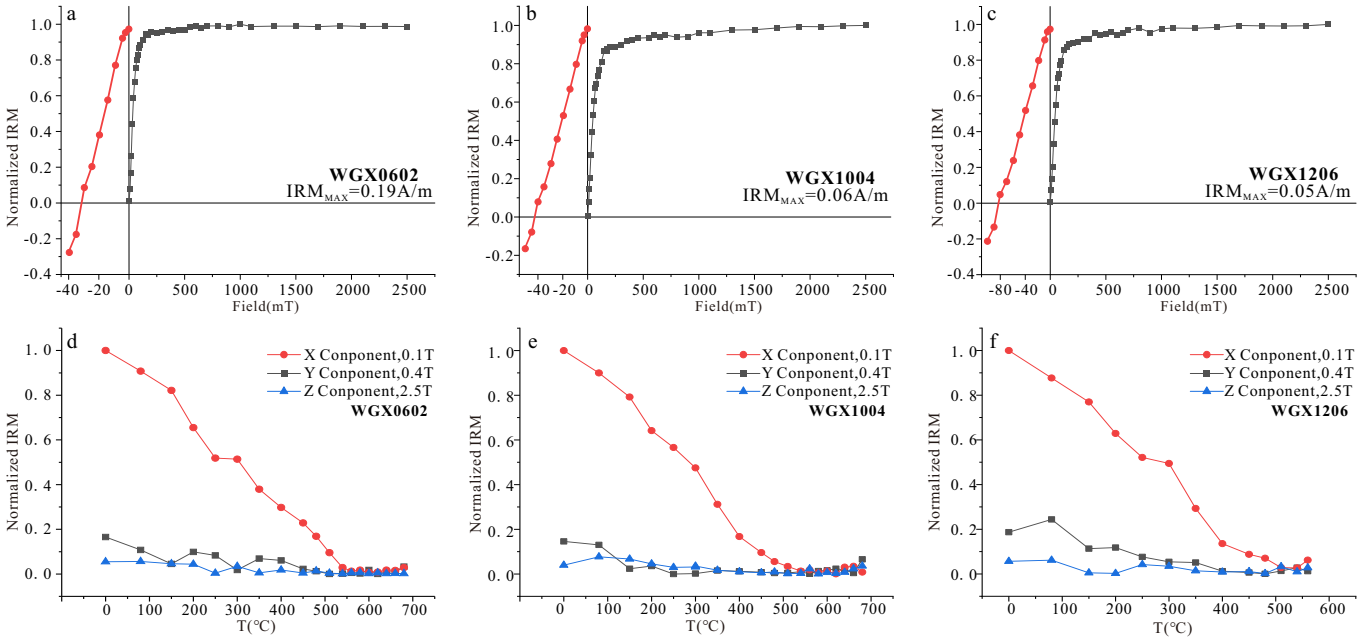
a
Normalized IRM
Field(mT)
WGX0602
IRM$_{MAX}$=0.19A/m
b
Normalized IRM
Field(mT)
WGX1004
IRM$_{MAX}$=0.06A/m
c
Normalized IRM
Field(mT)
WGX1206
IRM$_{MAX}$=0.05A/m
d
Normalized IRM
T(℃)
X Conponent,0.1T
Y Conponent,0.4T
Z Conponent,2.5T
WGX0602
e
Normalized IRM
T(℃)
X Conponent,0.1T
Y Conponent,0.4T
Z Conponent,2.5T
WGX1004
f
Normalized IRM
T(℃)
X Conponent,0.1T
Y Conponent,0.4T
Z Conponent,2.5T
WGX1206

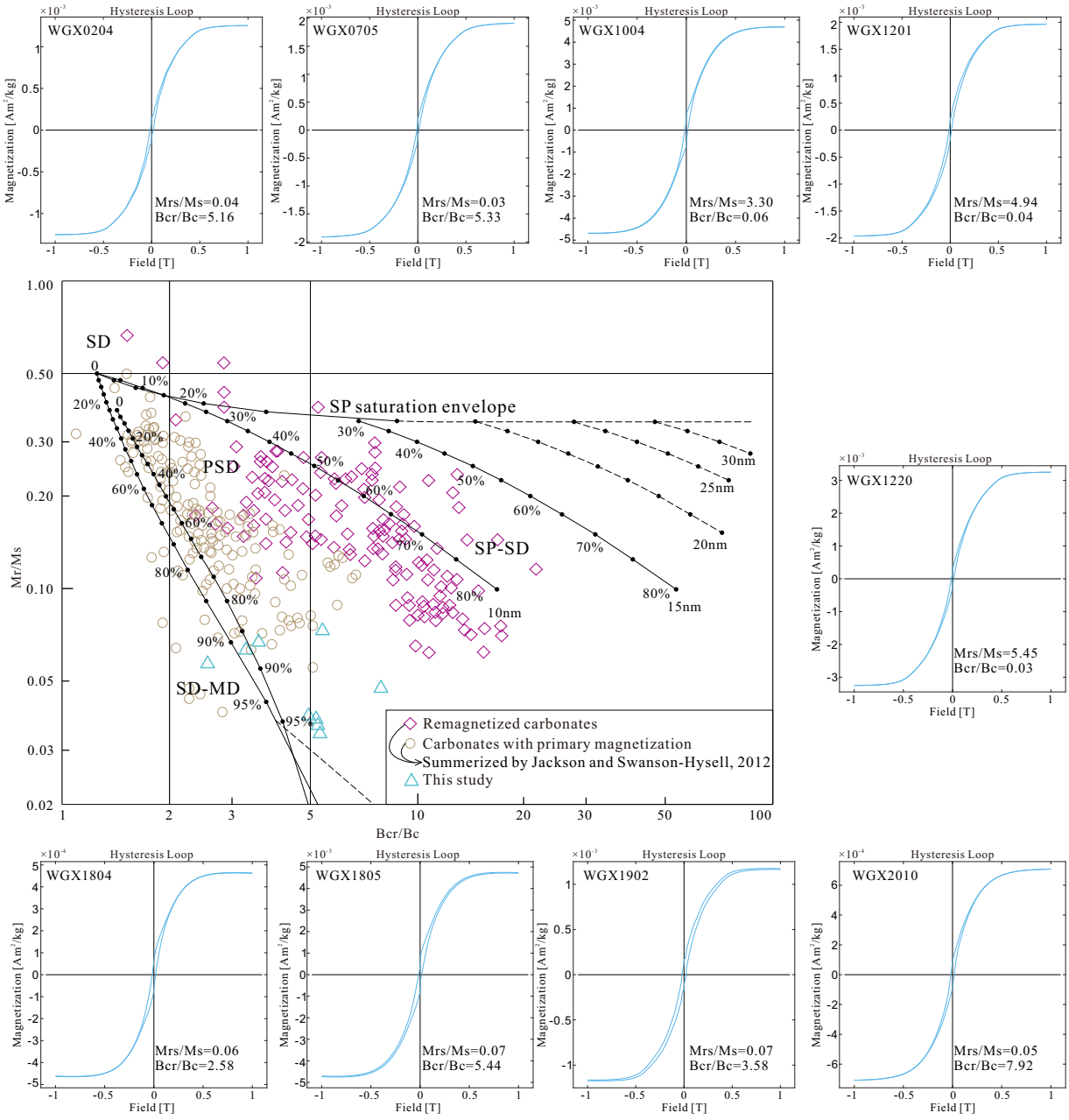
Hysteresis Loop
WGX0204
Mrs/Ms=0.04
Bcr/Bc=5.16
WGX0705
Mrs/Ms=0.03
Bcr/Bc=5.33
WGX1004
Mrs/Ms=3.30
Bcr/Bc=0.06
WGX1201
Mrs/Ms=4.94
Bcr/Bc=0.04
Magnetization [Am²/kg]
Field [T]
SD
PSD
SD-MD
SP saturation envelope
SP-SD
30nm
25nm
20nm
15nm
10nm
Mr/Ms
Bcr/Bc
Remagnetized carbonates
Carbonates with primary magnetization
Summerized by Jackson and Swanson-Hysell, 2012
This study
WGX1220
Mrs/Ms=5.45
Bcr/Bc=0.03
WGX1804
Mrs/Ms=0.06
Bcr/Bc=2.58
WGX1805
Mrs/Ms=0.07
Bcr/Bc=5.44
WGX1902
Mrs/Ms=0.07
Bcr/Bc=3.58
WGX2010
Mrs/Ms=0.05
Bcr/Bc=7.92

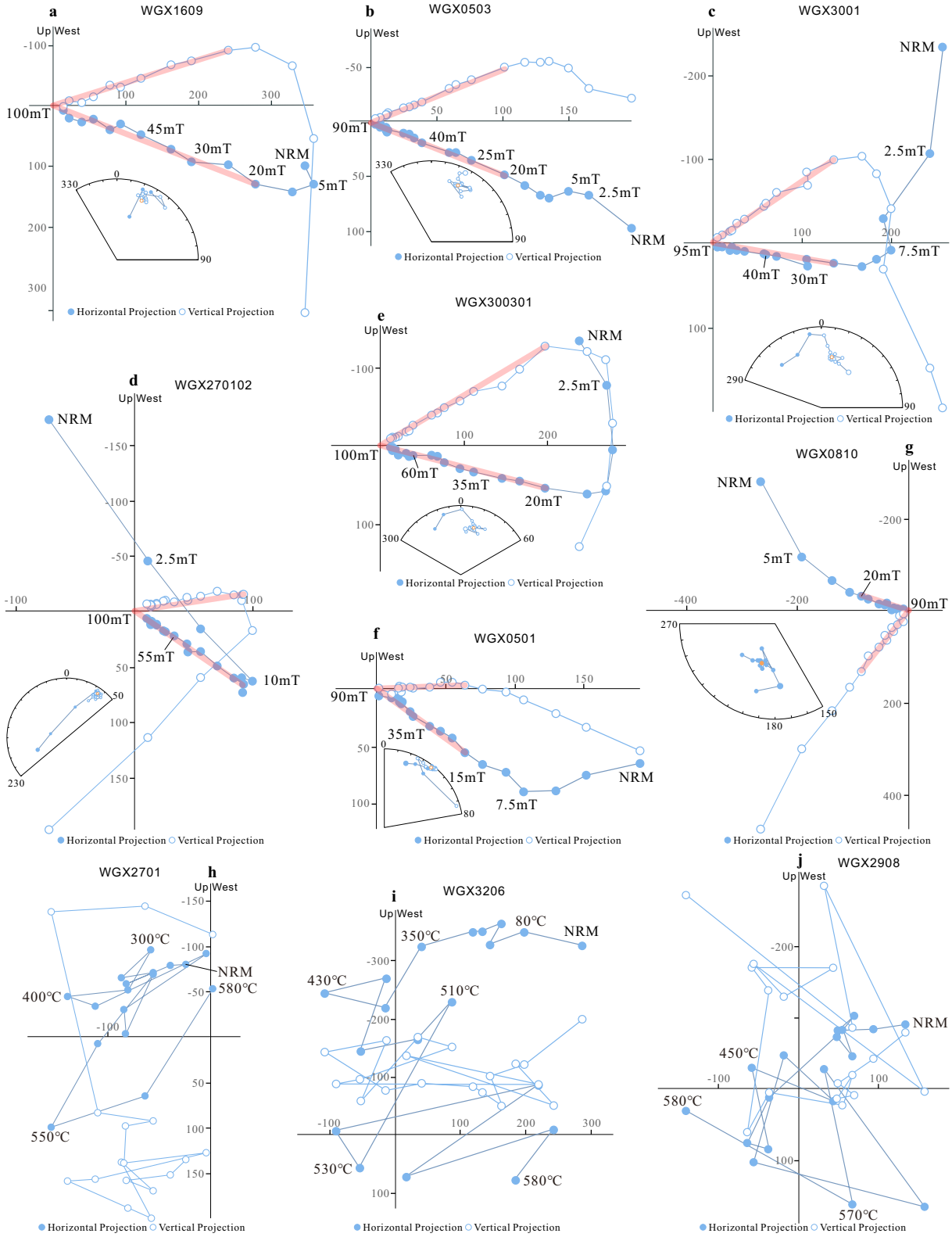
a
WGX1609
Up
West
100mT
45mT
30mT
20mT
NRM
5mT
Horizontal Projection
Vertical Projection
b
WGX0503
90mT
40mT
25mT
20mT
5mT
2.5mT
NRM
c
WGX3001
NRM
2.5mT
95mT
40mT
30mT
7.5mT
d
WGX270102
NRM
2.5mT
100mT
55mT
10mT
e
WGX300301
NRM
2.5mT
100mT
60mT
35mT
20mT
f
WGX0501
90mT
35mT
15mT
7.5mT
NRM
g
WGX0810
NRM
5mT
20mT
90mT
h
WGX2701
300℃
NRM
580℃
400℃
550℃
i
WGX3206
350℃
80℃
NRM
430℃
510℃
530℃
580℃
j
WGX2908
NRM
450℃
580℃
570℃

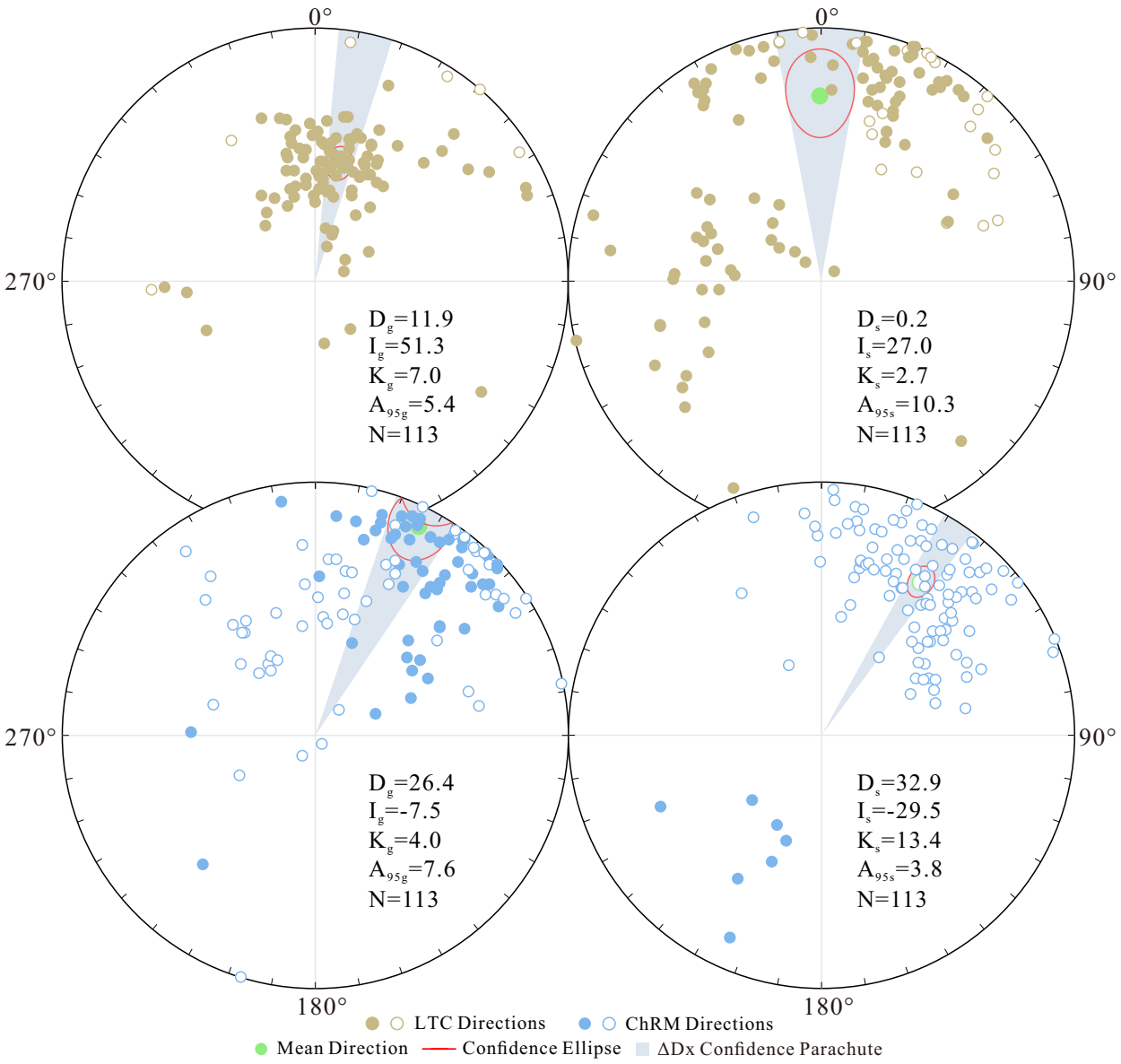
0°
270°
90°
180°
D_g=11.9
I_g=51.3
K_g=7.0
A_{95g}=5.4
N=113
D_s=0.2
I_s=27.0
K_s=2.7
A_{95s}=10.3
N=113
D_g=26.4
I_g=-7.5
K_g=4.0
A_{95g}=7.6
N=113
D_s=32.9
I_s=-29.5
K_s=13.4
A_{95s}=3.8
N=113
LTC Directions
ChRM Directions
Mean Direction
Confidence Ellipse
ΔDx Confidence Parachute

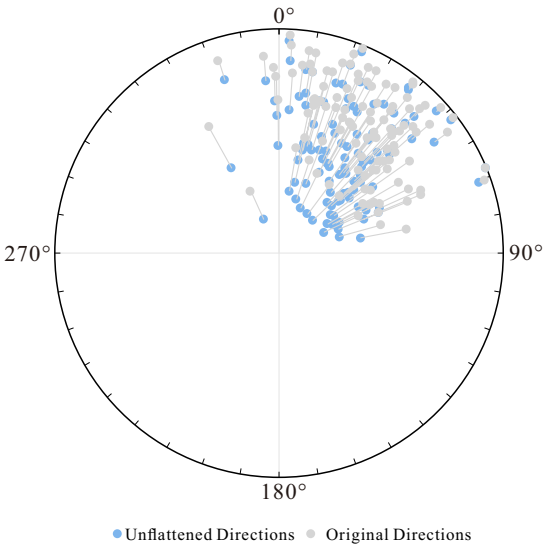
0°
270°
90°
180°
Unflattened Directions
Original Directions

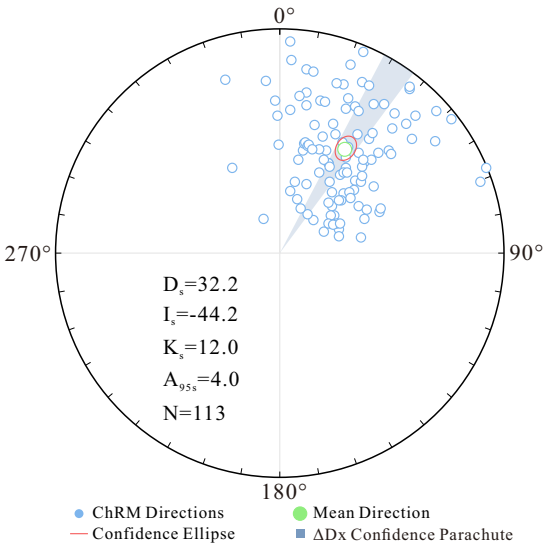
0°
270°
90°
180°
D$_s$=32.2
I$_s$=-44.2
K$_s$=12.0
A$_{95s}$=4.0
N=113
ChRM Directions
Mean Direction
Confidence Ellipse
ΔDx Confidence Parachute

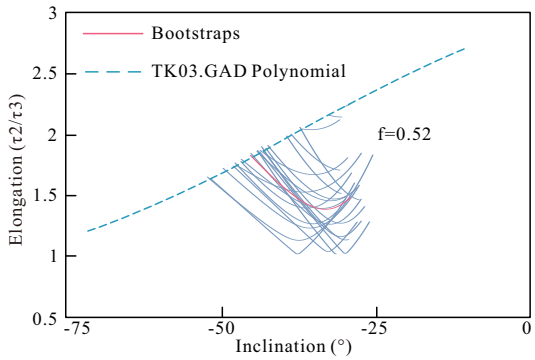
Bootstraps
TK03.GAD Polynomial
f=0.52
Elongation (τ2/τ3)
Inclination (°)
3
2.5
2
1.5
1
0.5
-75
-50
-25
0

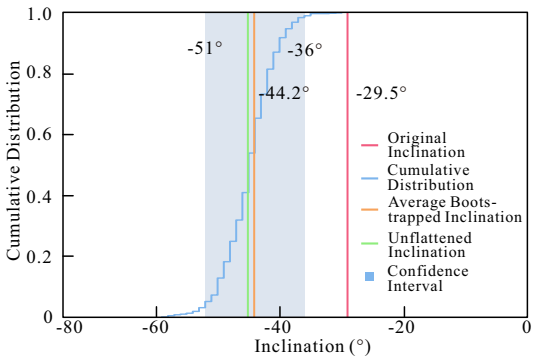
-51°
-36°
-44.2°
-29.5°
Original Inclination
Cumulative Distribution
Average Boots-trapped Inclination
Unflattened Inclination
Confidence Interval
Cumulative Distribution
Inclination (°)
1.0
0.8
0.6
0.4
0.2
0
-80
-60
-40
-20
0

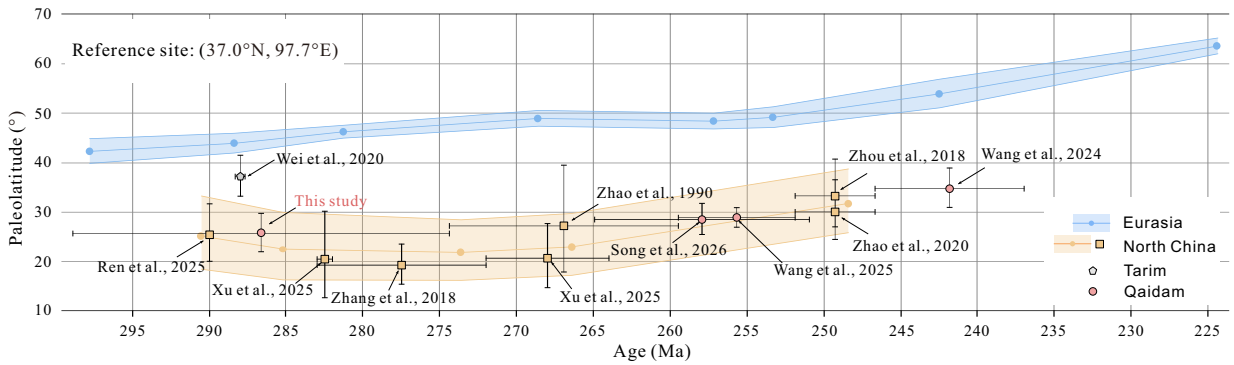
Reference site: (37.0°N, 97.7°E)
Paleolatitude (°)
Age (Ma)
70
60
50
40
30
20
10
295
290
285
280
275
270
265
260
255
250
245
240
235
230
225
Wei et al., 2020
This study
Ren et al., 2025
Xu et al., 2025
Zhang et al., 2018
Zhao et al., 1990
Xu et al., 2025
Song et al., 2026
Wang et al., 2025
Zhou et al., 2018
Zhao et al., 2020
Wang et al., 2024
Eurasia
North China
Tarim
Qaidam

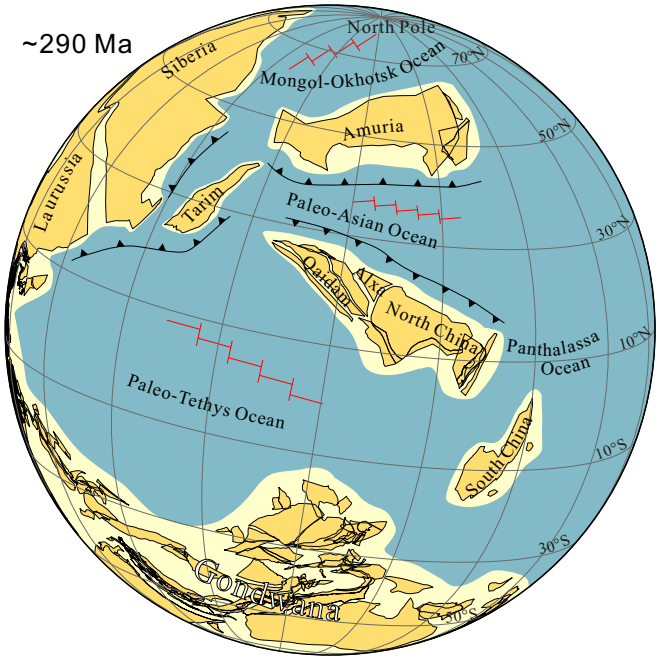
~290 Ma
North Pole
Siberia
Mongol-Okhotsk Ocean
70°N
Amuria
50°N
Laurussia
Tarim
Paleo-Asian Ocean
30°N
Qaidam
Alxa
North China
Panthalassa Ocean
10°N
Paleo-Tethys Ocean
10°S
South China
30°S
Gondwana
50°S

Supplementary Materials for

Was there an ocean between the North China-Qaidam and Tarim blocks connecting the Mongol-Okhotsk and Paleo-Tethys oceans?

Teng Wang[a], Yanan Zhou[a*], Douwe J.J. van Hinbergen[b*], Mark J. Dekkers[b], Zhenwei Chen[a], Ruiyang Chai[a, b], Dongmeng Zhang[a], Bitian Wei[c], Xin Cheng[a], Hanning Wu[a], Yunpeng Dong[a*]

a. State Key Laboratory of Continental Evolution and Early Life, Department of Geology, Northwest University, Xi'an, China

b. Department of Earth Science, Utrecht University, Utrecht, Netherlands

c. State Key Laboratory of Lithospheric and Environmental Coevolution, Institute of Geology and Geophysics, Chinese Academy of Sciences, Beijing 100029, China

***Corresponding authors:**

Yanan Zhou, zhouyanan@nwu.edu.cn

Douwe van J.J. Hinbergen, D.J.J.vanHinsbergen@uu.nl

Yunpeng Dong, dongyp@nwu.edu.cn

This file includes:

Figure S1-S4

Table S1–S2

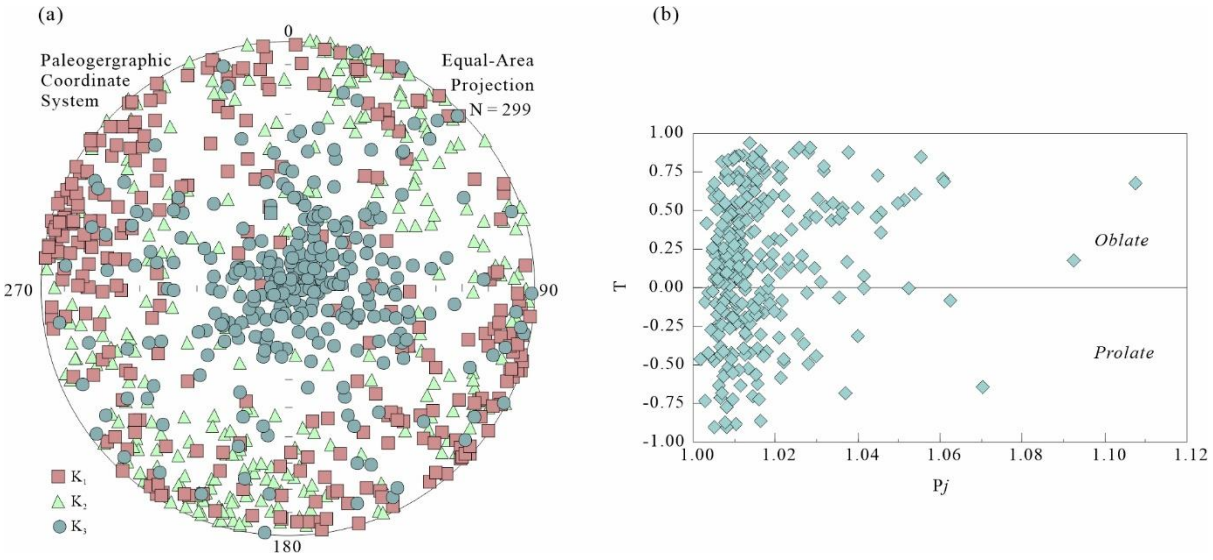

Figure S1. Anisotropy of magnetic susceptibility (AMS) of samples from Zhabusagaxiu Formation limestones. (a) Stereographic projections of principal susceptibility axes of K_{max}, K_{int}, and K_{min} in the paleogeographic coordinate system, (b) Corrected AMS degree (P*j*) versus AMS shape parameter (T).

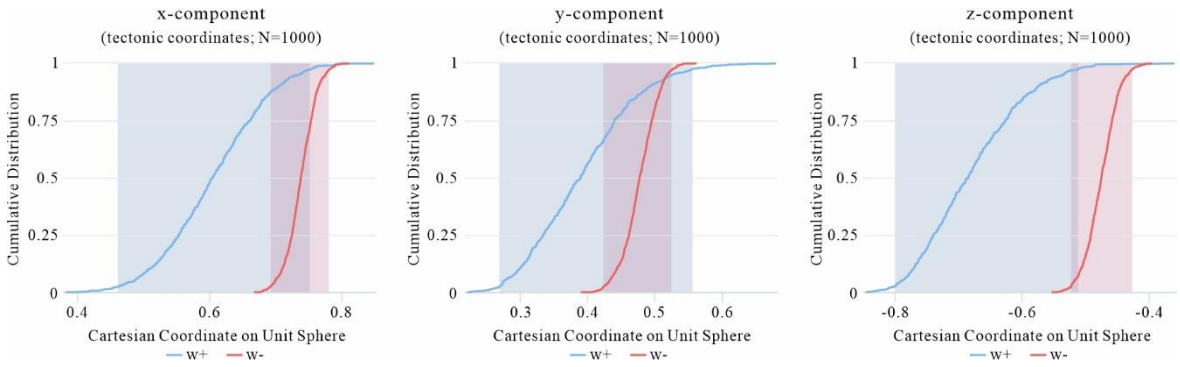

Figure S2. The bootstrapped reversal test of the Zhabusagaxiu Formation. The results show that the X, Y, and Z axes of the mean direction of the ChRMs coincide within confidence, indicating a positive reversal test.

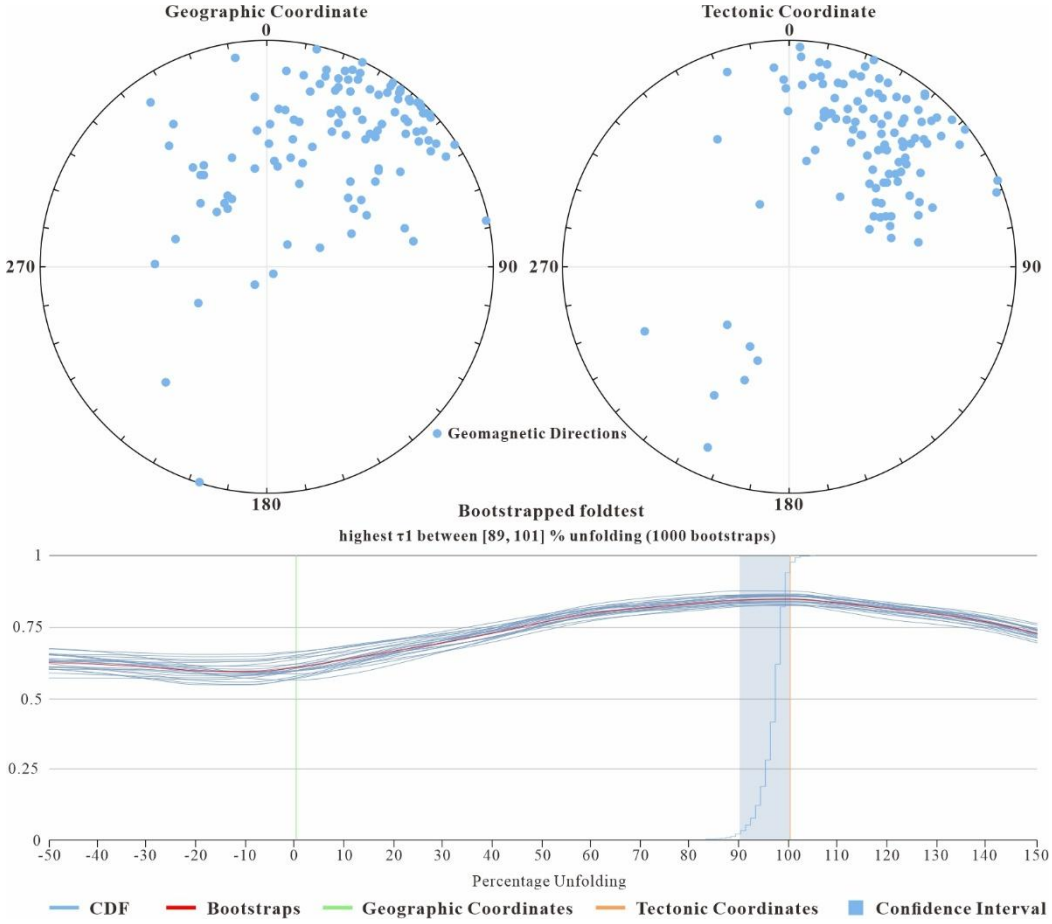

Figure S3. The bootstrapped fold test of Tauxe and Watson (1994), the precision parameter reaches a maximum between 89-101% unfolding during the progressive unfolding, indicating a positive fold test.

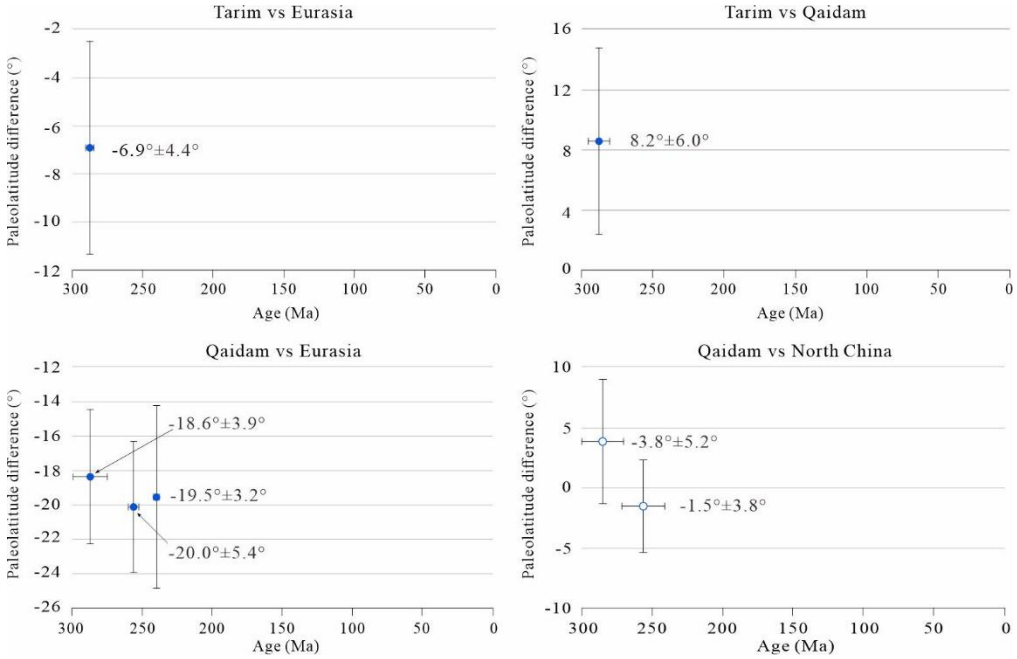

Figure S4. (a) The relative paleolatitudinal difference between the Tarim Basin versus Eurasia; (b) The relative platitudinal difference between the Tarim Basin versus Qaidam Basin; (c) The relative paleotitudinal difference between the Qaidam Basin versus Eurasia; (d) The relative paleotitudinal difference between the Qaidam Basin versus the North China Block. Open circles indicate data points that are statistically are not significantly different from zero. Errors bars indicate the age uncertainty range and 95% confidence regions.

Table S1. Paleomagnetic results of each sample of the Zhabusagaxiu Formation

Name	Declination	Inclination	Core azimuth	Core dip	Bedding strike	Bedding dip	MAD	Number steps	Range of component (mT)
107	226.16	59.4	318	32	303	27	14.1	13	25-95
705	46.29	-33.19	350	25	303	36	5.9	11	20-85
803	47.97	-47.11	4	45	312	45	6.5	7	25-55
908	70.44	-2.9	208	30	124	41	7.4	14	25-90
20702	12.73	-46.24	246	6	284	45	3.6	17	25-110
280101	9.57	-15.6	313	29	139	34	7.9	10	25-70
300302	13.2	-32.77	294	25	136	47	3.9	19	20-120
300501	20.82	-11.01	299	33	136	47	10.5	13	25-90
5005	44.35	-10.94	41	63	294	24	6	11	20-70
704	35.12	-39.71	343	27	303	36	7.8	13	20-75
708	32.99	-25.78	350	25	303	36	9.4	14	20-85
815	15.22	-23.88	20	47	312	45	7	12	25-80
1901	359.68	-31.97	298	14	224	51	7.2	18	20-75
2510	18.72	-11.41	333	25	231	53	10.6	6	20-85
200102	8.55	-9.73	298	28	214	56	12.4	12	25-80
201002	204.16	13.77	289	34	214	56	3.1	18	30-130
250401	59.47	-37.85	307	45	231	53	6.2	9	25-65
251101	68.26	-38.14	332	37	231	53	6.6	13	25-80
270101	38.49	-3.84	300	26	125	87	2.7	15	25-95
270102	35.24	-10.51	310	33	125	87	3.5	16	25-100
300502	65.07	-57.88	299	33	226	47	7.5	11	25-75
0706	38.11	-32.02	352	26	303	36	6.1	14	25-90
0709	46.63	-18.99	348	25	303	36	8.5	11	25-75
0807	68.12	-50.19	10	48	312	45	6.7	9	25-65
50401	25.69	-8.68	49	18	294	24	7.3	16	25-110
50501	43.16	-26.48	41	53	294	24	7.2	9	20-60

50801	44.55	-21.51	27	55	294	24	6.5	7	20-50
50802	38.27	-20.44	27	55	294	24	9.1	8	25-55
WGX07-0	24.78	-30.22	342	30	303	36	9.3	9	25-70
WGX08-1	13.01	-30.49	34	45	312	45	5.8	7	25-60
WGX19-0	43.76	-27.86	296	28	134	51	13.2	4	55-80
WGX30-0	13.09	-30.04	303	38	136	47	9.1	10	25-90
WGX0204	67.60	-31.86	256	27	284	45	10.0	6	30-60
WGX0403	48.48	-19.34	302	-1	315	54	13.5	6	25-60
WGX0407	48.06	-3.18	319	-2	315	54	1.6	4	20-35
WGX0501	38.17	-3.44	354	41	294	24	4.7	11	25-90
WGX0703	29.93	-25.58	349	34	303	36	7.9	10	25-90
P1Z1806	9.61	-50.71	50	20	310	42	14.9	5	20-70
P1Z0102	49.86	-35.52	90	12	309	48	12.0	9	20-110
P1Z0107	37.98	-18.39	80	12	309	48	6.4	8	20-90
P1Z0301	27.21	-15.00	69	24	310	42	8.7	7	30-90
P1Z0302	14.94	-16.90	67	21	310	42	13.5	6	20-70
P1Z0303	4.30	-20.75	63	16.5	310	42	7.4	6	20-90
P1Z2006	37.69	-35.28	60	23	310	42	10.9	8	20-90
WGX0303	47.30	-39.45	339	24	310	36	5.3	15	20-130
WGX0508	49.10	-31.75	144	12.5	314	67	14.6	7	20- 60
WGX0904	10.65	-10.05	323	21	313	57	13.1	12	25-130
WGX0306	55.75	-48.91	33	43	310	36	4.5	17	10-130
WGX1608	28.31	-8.58	52	52	138	37	4.9	15	20-130
WGX0405	54.78	-29.21	234	30	315	58	10.7	14	20-130
WGX16032	24.90	-16.49	44	53	138	37	5.1	11	20-90
WGX0901-2	38.85	-33.69	325	14	313	57	14.1	6	30-60
WGX1609	22.59	-21.84	52	55	138	37	4.9	12	20-100

WGX09061	28.54	-33.97	338	3	313	57	11.4	9	20-80
WGX0309	44.15	-47.43	48	42	310	36	11.0	11	20-100
WGX1503	330.89	-35.83	270	31	90	26	2.2	11	20-90
WGX1601	29.12	-15.78	44	53	138	37	4.1	11	20-90
25WGX04	52.13	-1.71	324	-7	315	54	6.1	8	20-60
25WGX06	44.58	-24.44	23	45	294	24	4.4	9	25-65
25WGX06	49.41	-12.44	24	49	294	24	3.9	9	20-60
0605	39.54	-10.86	24	48	294	24	9.4	8	20-55
0802	29.02	-34.00	359	44	312	454	13.1	15	20-90
2501	21.33	-30.79	298	45	141	53	5.5	11	20-70
50301	25.27	-24.18	41	59	294	24	1.9	15	20-90
121401	14.74	-31.06	314	10	139	74	9.2	11	20-70
300102	11.86	-36.59	303	38	136	47	3.8	16	20-95
300702	7.34	-16.85	299	35	136	47	7.2	12	25-80
0702	34.83	-29.01	346	30	303	36	5.8	13	25-80
0205	25.25	-33.51	248	0	284	45	5.2	14	25-90
0805	49.60	-42.48	10	50	312	45	11.3	10	25-70
0902	79.41	-41.52	196	24	2144	41	12.7	8	45-80
2202	53.45	-50.44	225	41	227	54	8.4	14	25-90
2212	335.63	-65.26	241	47	227	54	8.3	9	25-65
2505	62.26	-50.10	303	46	231	53	7.5	10	25-70
2512	42.38	-14.21	335	27	231	53	7.3	11	25-70
200102	22.52	-1.62	298	38	214	56	7.3	16	25-100
200302	20.88	-5.84	304	27	214	56	9.5	13	25-90
201001	49.07	-37.63	289	26	214	56	12.8	14	30-95
300301	15.45	-30.28	294	25	136	47	2.6	17	20-100
300701	359.17	-22.42	299	35	136	47	4.3	11	40-90
0801	59.27	-53.94	357	42	312	45	9.4	13	30-90

0806	52.17	-38.78	0	0	270	0	11.6	9	25-70
1004	36.57	-58.55	335	27	310	85	7.7	5	30-50
2102	355.65	-12.97	313	13	124	56	6.5	7	25-55
2409	46.91	-30.26	316	5	223	41	9.5	10	25-70
2503	74.63	-51.13	299	34	231	53	7.9	13	25-85
300402	16.70	-16.94	293	26	136	47	6.9	9	25-65
0206	17.75	-31.72	244	5	284	45	4.2	14	20-85
0409	44.75	-7.95	325	-3	315	54	8.1	14	20-85
0808	20.40	-26.63	10	50	312	45	13.9	10	25-70
0809	48.63	-43.22	8	52	312	45	6.6	12	25-80
0810	32.47	-11.97	13	54	312	45	13.2	12	25-80
0811	33.38	-21.20	21	60	312	45	12.9	13	20-80
20701	26.49	-38.57	246	6	284	45	3.6	17	20-100
30101	10.50	-18.83	306	17	165	84	11.7	8	25-60
50302	38.35	-25.47	49	59	294	24	6.9	14	20-85
50402	54.46	-8.30	49	58	294	24	8.6	12	25-80
280102	2.94	-3.10	313	29	139	34	10.8	12	25-80
0602	42.22	-26.19	33	43	294	24	7.4	9	25-65
0804	61.67	-51.97	5	43	312	45	7.9	12	25-80
1005	40.07	-33.15	336	44	310	59	5.6	5	20-40
1216	40.79	-42.81	276	54	139	74	14.7	9	40-80
1219	3.51	-7.98	312	43	139	74	8.8	5	25-45
1805	342.64	-10.87	320	26	131	54	12.1	11	25-75
1806	358.52	-18.38	322	2	131	54	10.9	12	25-80
2507	63.78	-48.32	304	40	231	53	8.6	9	25-70
240402	67.52	-0.21	330	-5	133	41	10.2	8	25-60
251102	63.59	-35.79	332	37	231	53	12.8	7	25-55
WGX0601	210.30	34.82	161	18	132	73	3.5	12	15-100

WGX0608	201.29	45.49	165	19	132	73	4.5	17	10-130
WGX1401	246.02	31.02	232	26	110	34	1.3	17	10-130
WGX0704	205.89	57.65	159	31	132	73	7.9	9	20-70
WGX0810	198.20	54.05	164	28	132	73	4.7	12	20-100

MAD= maximum angular deviation

Table S2 Compilation of Permo-Triassic Palaeomagnetic Poles from the Qaidam, North China, and Tarim (reference site: 37.0°N, 97.7°E)

Name	Age	Min_age	Max_age	Slat	Slon	N	K	A95	Plat	Plon	Mdec	Minc	Lithology	f	Paleolatitude	Reference
Qaidam	239.3	237.0	241.5	36.5	98.3	28	44.4	4.1	57.7	178.9	39.5	54.0	V		34.7	*(Wang et al., 2024)*
Qaidam	255.7	251.9	259.5	37.5	99.1	199	24.7	2.1	77.6	332.8	348.7	47.0	C	0.68	28.8	*(Wang et al., 2025)*
Qaidam	258.0	251.0	265.0	36.1	94.9	39	54.2	3.1	82.0	274.9	0.3	46.1	V		28.3	*(Song et al., 2026)*
Qaidam	282.2	274.4	289.9	37.0	97.7	113	12.0	4.0	-17.4	67.8	32.2	-44.2	L	0.52	26.0	*This study*
NorthChina	249.3	246.7	251.9	36.0	112.4	15	32.5	6.8	53.3	16.5	318.5	42.0	C	0.6	33.0	*(Zhou et al. ,2018)*
NorthChina	249.3	246.7	251.9	40.8	118.5	21	28.6	6.0	53.7	9.6	322.4	39.0	C	0.48	30.0	*(Zhao et al., 2020)*
NorthChina	290.0	290.0	290.0	42.5	119.5	21	31.3	5.8	41.1	11.6	311.8	29.0	V		25.3	*(Ren et al., 2025)*
NorthChina	267.0	259.5	274.4	43.2	119.0	14	15.2	10.6	75.6	339.2	347.5	46.8	V		27.1	*(Zhao et al., 1990)*
NorthChina	274.5	266.0	283.0	42.0	114.0	24	54.4	4.1	66.1	328.2	346.1	36.6	V		19.2	*(Zhang et al., 2018)*
NorthChina	268.0	264.0	272.0	39.6	101.1	11	29.2	8.6	49.8	355.9	317.6	36.7	V\C		20.6	*(Xu et al., 2025)*
NorthChina	282.5	282.0	283.0	39.6	101.1	17	31.8	6.4	40.2	5.2	306.0	36.0	V		20.4	*(Xu et al., 2025)*
Tarim	287.6	284.9	290.3	41.0	80.0	51	24.2	4.1	50.0	170.4	47.5	48.5	V\C		37.1	*(Wei et al., 2020)*

Min_age/Max_age = lower and upper boundaries of age uncertainty range (in Ma); Slat/Slon = latitude and longitude of (mean) sampling location; N = number of paleomagnetic sites used to compute the paleopole; K=Fisher (1953) precision parameter of the distribution of virtual geomagnetic poles (VGPs); A95 = radius of the 95% confidence circle about the paleopole; Plat/Plon = paleopole latitude and longitude; Mdec/Minc = mean declination and inclination; f = flattening factor (only for sedimentary data); V=volcanic rock; C= clastic rock; L=limestone.

References From the Supporting Information

Ren, Q., Zhang, S., Hou, M., Zheng, D., Wu, H., Yang, T., Li, H., Chen, A., Ogg, J.G., 2025. Continental drift triggered the Early Permian aridification of North China. Nat. Commun. 16, 384. https://doi.org/10.1038/s41467-024-55804-8

Song, P., Ding, L., Zhang, L., Wu, C., Duan, X., Yue, Y., Xie, J., 2026. Defining the main Paleo-Tethys suture in Tibet: first Permian paleomagnetic insights from the Eastern Kunlun Range. Earth Planet. Sci. Lett. 681, 119925. https://doi.org/10.1016/j.epsl.2026.119925

Wang, B., Huang, B., Yang, Z., Zhang, G., Liu, X., Duan, L., Armstrong, R.A., Meng, Q., 2024. Palaeomagnetic results from Early Mesozoic strata in the Qaidam Basin and their implications for the formation of the Northern China Domain. Geophys. J. Int., 236 (3), 1621-1635. https://doi.org/10.1093/gji/ggad496

Wang, T., Zhou, Y., van Hinsbergen, D.J.J., Sun, J., Cheng, X., Chai, R., Xu, S., Wang, P., Wu, H., 2025. Paleomagnetic evidence for a Late Permian Qaidam–North China connection, and the cryptic final Mesozoic intra-Asian suture. J. Geophys. Res. Solid Earth 130 (8), e2025JB031123. https://doi.org/10.1029/2025JB031123

Wei, B., Yang, X., Cheng, X., Domeier, M., Wu, H., Kravchinsky, V.A., Zhou, Y., Jiang, N., Wu, Y., Huo, F., 2020. An absolute paleogeographic positioning of the early Permian Tarim large igneous province. J. Geophys. Res. Solid Earth 125 (5), e2019JB019111. https://doi.org/10.1029/2019JB019111

Xu, W., Song, B., Shi, J., Li, Y., Wang, B., Ye, X., Han, X., Xu, H., Zhang, Y., Zhang, H., Sun, Z., 2025. New Permian paleomagnetic and geochronologic results from the Alxa Block: constraints on its tectonic affinity and the closure of Paleo-Asian Ocean. Geophys. Res. Lett. 52 (20), e2025GL116752. https://doi.org/10.1029/2025GL116752

Zhang, D., Huang, B., Zhao, J., Meert, J.G., Zhang, Y., Liang, Y., Bai, Q., Zhou, T., 2018. Permian paleogeography of the eastern CAOB: paleomagnetic constraints from volcanic rocks in central eastern Inner Mongolia, NE China. J. Geophys. Res. Solid Earth 123 (40), 2559-2582. https://doi.org/10.1002/2018JB015614

Zhao, P., Appel, E., Xu, B., 2020. An inclination shallowing-corrected Early Triassic paleomagnetic pole for the North China Craton: implication for the Mesozoic geography of Proto-Asia. J. Geophys. Res. Solid Earth 125 (10), e2020JB019489. https://doi.org/10.1029/2020JB019489

Zhao, X., Robert, S.C., Zhou, Y., Wu, H., Wang, J., 1990. New paleomagnetic results from northern China: collision and suturing with Siberia and Kazakhstan. Tectonophysics 181 (1-4), 43-81. https://doi.org/10.1016/0040-1951(90)90008-V

Zhou, T.H., Huang, B.C., Jia, S.F., Liang, Y.L., Zhang, D.H., Zhao, Q., Zhang, Y., Yan, Y.G., 2018. Paleomagnetic inclination shallowing in Lower Triassic Liujiagou Formation from Qinshui Basin, North China Block. Acta Sci. Nat. Univ. Pekin., 54 (3), 521-534. (In Chinese with English abstract)